R. & M. No. 3501

MINISTRY OF TECHNOLOGY

AERONAUTICAL RESEARCH COUNCIL

REPORTS AND MEMORANDA

Measurements of Skin Friction on a Cambered Delta Wing at Supersonic Speeds

By K. G. WINTER and K. G. SMITH

LONDON: HER MAJESTY'S STATIONERY OFFICE
1967
PRICE £1 0*s.* 0*d.* NET

Measurements of Skin Friction on a Cambered Delta Wing at Supersonic Speeds

By K. G. WINTER and K. G. SMITH

Reports and Memoranda No. 3501*
August, 1965

Summary.

The measurements, using razor blade surface pitot tubes, show that the relatively mild pressure gradients and streamline convergence on the wing have a large effect on local skin friction. Application of the boundary-layer momentum equation suggests that the change in skin friction arises directly from changes in the boundary-layer profile. Despite large variations the total skin-friction drag of the wing is within 10 per cent of that of a flat plate.

LIST OF CONTENTS

*Replaces R.A.E. Tech. Report No. 65 181—A.R.C. 27 559.

1. *Introduction.*

Reference 1 describes a simple method of measuring skin friction at supersonic speeds using pieces of razor blade to convert static pressure holes into surface pitot tubes; two examples of the use of the technique on wind-tunnel models are given. This report describes a further experiment on a cambered delta-wing model with rather more comprehensive measurements of skin friction. A study of the flow field round the model at one condition is included. The measurements were made during 1959.

On the wing upper surface the camber design results in regions with mild adverse pressure gradients. In these regions the skin friction falls to values as low as half the turbulent flat plate value. Application of the boundary-layer momentum equation between two stations on the wing, using the measured flow directions, shows that the low values of skin friction are not consistent with a flat-plate relationship to momentum thickness.

To study this problem further and to extend the work generally on the behaviour of boundary layers in pressure gradients and non-parallel flow, a waisted body has been designed which has pressure gradients of the same magnitude as on the wing. Boundary layer profiles were also measured. It is shown in Refs. 2 and 3 for Mach numbers up to 2, that the combined effect of adverse pressure gradient and streamline convergence is to produce profiles with a large wake component, and consequent low skin-friction coefficient.

2. *Model*, Figs. 1 and 2.

The model used was a delta wing of aspect ratio 4/3 with Lord V type of thickness distribution. The centreline chord was 60 in. The maximum thickness: chord ratio on the model centreline was 8·43 per cent and the thickness tapered linearly spanwise, i.e. the basic thickness distribution was of rhombic cross-section. The camber and twist were designed by linear theory[4] to give attached flow along the leading edges at a lift coefficient of 0·1 and a Mach number of 2.1. This condition is referred to as the design point. Some thickening of the wing towards the tips was added to the nominal shape to increase the stiffness of the wing which was manufactured from reinforced plastics. The equations of the camber surface and the thickness distribution are given in the Appendix. The centre section at the rear of the wing was distorted to accommodate the supporting sting. On each surface twenty-three pressure tubes were provided arranged along five chordwise lines in one half of the wing at spanwise positions of 1, 5, 8, 11·5 and 15 in. By appropriate drilling, any position along each of the lines could be selected. Two sets were in fact used during the tests.

3. *Test Procedures.*

The model was tested in the R.A.E. 8 ft × 8 ft wind tunnel at Reynolds numbers of 10×10^6 based on centreline chord at Mach numbers of 1·5, 2·1 and 2·6, and also at a Reynolds number of 5×10^6 at $M = 2{\cdot}1$. The strength of the model limited the maximum incidence to 6, 8 and 10 degrees respectively at M 1·5, 2·1 and 2·8 for a Reynolds number of 10×10^6. For each set of pressure holes static pressures were measured first and surface pitot pressures obtained in a subsequent run after pieces of razor blade had been secured over the pressure holes as described in Ref. 1. The razor blades were mounted with their edges normal to the freestream direction. The razor blade heights were measured with a depth microscope when the wing was removed from the tunnel. For these tests boundary layer transition was not fixed.

In order to obtain overall forces, tests were also made with the model mounted on an internal balance. For these tests a transition trip of 100 grade carborundum (approximately 0·005 in.), which extended from 0·1 in. to 0·6 in. measured along a normal to the leading edge, was attached to the model by means of paint.

To help in interpreting the skin-friction results explorations of the flow field round the model were made in planes normal to the longitudinal axis of the model at stations 40 in. and 48 in. from the nose $\left(\frac{x}{c_0} = 0{\cdot}667 \text{ and } 0{\cdot}8\right)$. In each plane the survey covered a band extending between one and two inches from the wing surface round half the wing. The probe used was a 60 degree conical five tube yawmeter

of 0·1 in. diameter. The tests were made before the self-aligning probe described in Ref. 5 was developed; the equipment carrying the probe was however the same as described there. The probe was aligned with the model longitudinal axis. Local flow directions and local Mach numbers were obtained from the pressures measured at the five holes using an extensive calibration in the manner described by Centolanzi[6].

4. *Accuracy.*

Analysis of the pressure measuring techniques employed, made subsequent to the tests, has shown that the datum pressure to which the pressure coefficients are referred is probably in error. The effect of this could be to increase the pressure coefficients given by up to 0·01. Reading errors on the individual measurements should not exceed $\pm 0{\cdot}005$ except at the lower Reynolds number. Possible errors in skin-friction coefficient (in addition to any uncertainty in the calibration curve[1] used) arising from reading errors are estimated to be about $\pm 0{\cdot}0003$ at a Reynolds number of 10×10^6 and $\pm 0{\cdot}0006$ at 5×10^6. Assuming a maximum crossflow of about 10 degrees the error in c_f due to misalignment of the razor blades with the local flow direction should not exceed 2 per cent. The scatter in some of the experimental results exceeds these estimates. This may be due to inaccurate positioning of the razor blades with respect to the static holes. Recent work has shown this to be more critical than was originally supposed. It is important, for the calibration given in Ref. 1 to hold, that the leading edge of the razor blade is over the leading edge of the pressure hole.

The errors introduced in integrating the pressure and skin-friction measurements to obtain the pressure and skin-friction contributions to axial force are difficult to assess. An estimate for the possible error in axial-force coefficient due to pressure is $\pm 0{\cdot}0005$ but the probable value is less than this unless there was serious distortion of the model under load. The possible error in axial-force coefficient due to skin friction should not exceed $\pm 0{\cdot}0001$.

For the total axial-force coefficient as measured by a balance the estimated possible error is $\pm 0{\cdot}0006$. This figure is composed of $\pm 0{\cdot}0003$ scatter apparent when the results, which are available for Mach numbers other than used here, are plotted as an incidence-Mach number carpet and a similar figure from possible reading error and balance calibration error. Improved techniques have reduced this error considerably in subsequent tests.

5. *Results.*

Figs. 3, 4, 5 and 6 give the basic results for skin friction and pressure coefficients. The distributions are plotted along chordwise lines at spanwise positions of 0·05, 0·25, 0·4, 0·575 and 0·75 times the semi-span. All coefficients are referred to freestream kinetic pressure. The flagged symbols indicate results from the second set of pressure holes. The same fairing lines are drawn through the pressure coefficients of Figs. 4 and 5, the results shown in which, differ only in Reynolds number.

The pressure distributions have a general character which does not change much with either Mach number or incidence. On the upper surface there is a favourable gradient up to about 50 per cent local chord followed by an adverse gradient up to about 80 per cent, and finally a favourable gradient to the trailing edge. The adverse gradient diminishes towards the tip and is absent at the station at 75 per cent semi-span. On the lower surface the pressure gradient is generally favourable up to about 70 per cent chord with an unfavourable gradient from there to the trailing edge. It should be remarked that all the pressure gradients are in fact small, the velocity perturbations not exceeding about 5 per cent. The effect of the camber at the leading edge is to give attached flow there at about 5 degrees incidence. For lower angles separation occurs on the lower surface and for larger angles on the upper surface, giving the usual suction peaks near the leading edge.

As a standard against which to compare the measurements, the broken lines have been drawn on the graphs of skin-friction distribution indicating estimates of flat-plate skin friction using freestream conditions. For these estimates a laminar boundary layer run of 1·5 million, followed by a transition region of 1 million with a linear rise of skin friction, has been assumed near the centreline, and a laminar run of 1 million with abrupt transition away from the centreline. The different assumptions on different parts of the wing were taken as being a possible interpretation of the measurements and of sublimation patterns on similar wings, though no such patterns are available for this wing. The different types of transition

could indicate the different types of mechanism as described by Cooke[7], namely Tollmien-Schlichting instability near the centreline and sweep instability away from the centre-line. The calculations used the charts of Smith[8] which are based on the formulae of Blasius for laminar boundary layers and of Prandtl-Schlichting for turbulent boundary layers with compressibility accounted for by the intermediate enthalpy concept.

The skin friction behaves similarly at all the test conditions. Near the model centreline $\left(\frac{y}{s_0} = 0{\cdot}05\right)$ for most conditions there is some laminar flow followed by a transition region. Transition is generally further forward than has been assumed in the estimates. On the upper surface following transition the skin friction decreases rapidly to a value about half that of the flat plate estimate at $\frac{x}{c_0} = 0{\cdot}75$, i.e. slightly upstream of the end of adverse pressure gradient. From $\frac{x}{c_0} = 0{\cdot}75$ to the trailing edge the skin friction increases again roughly to the flat-plate value. The same sort of pattern, though with a less pronounced dip in the skin friction, holds over the rest of the span. On the lower surface, where the pressure gradient is mainly favourable, the measurements follow more closely the estimate in the turbulent region but having somewhat lower values particularly at $M = 1{\cdot}5$*. The effect of reducing Reynolds number from 10 million to 5 million at $M = 2{\cdot}1$ (*compare* Figs. 4 and 5) does not change the distribution a great deal. Transition is further back but the transition Reynolds number is lower at the lower Reynolds number.

The detail of the experiment is not good enough to identify any local effects of the edge separations but there is a considerable reduction in the level of skin friction when separation occurs. For example at $M = 2{\cdot}1$ the skin-friction coefficient on the upper surface away from the wing centreline is much less at 8 degrees incidence than at zero incidence (*compare* Figs. 5a and 5f).

To illustrate further the effects of the pressure gradients on the skin friction, contours of constant pressure and constant skin friction at the design condition of the wing are shown for the upper surface in Fig. 7 and for the lower surface in Fig. 8. Considerable smoothing was necessary to obtain the skin-friction contours. The main point which the figures illustrate is in Fig. 7 where the contour of the low value of c_f of 0·001 can be seen to coincide approximately with the region of adverse pressure gradient.

The distributions of Figs. 3 to 6 have been integrated to obtain pressure and skin-friction axial-force coefficients. The integration was done numerically using a Weddle formula for each chordwise station taking values interpolated from the curves drawn. The chordwise integrals were integrated spanwise also numerically with multiplying coefficients derived by integration of a Lagrange interpolation formula. No corrections were made for the presence of the sting fairing. By subtracting the axial force due to normal pressure from the measured total axial force a total skin-friction axial force $(-C_{X_T})$ is obtained. The skin-friction axial force and that obtained by integration of the local measurements $(-C_{X_F})$ are shown in Figs. 9 to 12 and compared with flat-plate estimates for both fully turbulent flow and for flow with the laminar runs assumed in Figs. 3 to 6. The lack of accuracy in the experiments prevents any very firm conclusions being drawn but it is possible to make some tentative deductions by considering average values. The following Table gives average values of the axial-force coefficients taken for nominal incidences of 0, 2, 4 and 6 degrees at a Reynolds number of 10×10^6.

	M	1·5	2·1	2·6
Axial-force coefficient from balance minus pressure	$(-C_{X_T})$	0·0057	0·0044	0·0048
Turbulent estimate		0·0054	0·0048	0·0043
Difference		+0·0003	−0·0004	+0·0005
	Mean difference	+0·0001		

*More recent work on razor blade calibration shows that the calibration curve given in Ref. 1 holds only for Mach numbers above about 1·6. For Mach numbers between 1·6 and 0·8 there is a region of Mach number dependency of the calibration. Below $M = 0{\cdot}8$ a subsonic calibration holds.

	M	1·5	2·1	2·6
Axial-force coefficient from integrated skin friction	$(-C_{X_F})$	0·0043	0·0038	0·0036
Estimate with free transition		0·0047	0·0042	0·0038
Difference		−0·0004	−0·0004	−0·0002
	Mean difference	−0·0003		

It will be seen that the mean values of the axial-force coefficient from balance and pressures are higher than the turbulent flat-plate estimate at $M = 1{\cdot}5$ and 2·6, and lower at $M = 2{\cdot}1$. As remarked in Section 4 the force measurements exhibited a scatter of this nature of about $\pm 0{\cdot}0003$ in. $-C_X$ i.e. of the same order as shown in the Table. The mean value of the difference is $+0{\cdot}0001$. However no allowance has been made for the drag of the roughness band used as a boundary-layer trip. For a 60 grade band Evans[9] has estimated this to be 0·0032 times the ratio of the roughness band area to the reference area. Though his roughness was larger than used on this model it was distributed more sparsely and the same figure is probably applicable. This would give an increment in axial-force coefficient of 0·0003. Taking this into account the mean value for the difference between the measurements and the estimate would be $-0{\cdot}0002$. The corresponding figure for the integrated skin friction compared with the appropriate estimate is $-0{\cdot}0003$. It might therefore be fair to conclude that the skin-friction drag of the wing is lower than a flat-plate value by a little over 5 per cent.

The effect of reducing Reynolds number from 10×10^6 to 5×10^6 at $M = 2{\cdot}1$ is to produce an increase in the total skin friction (Figs. 11 and 12) rather than the approximately unchanged value estimated for constant transition Reynolds number. This implies that in fact there is a reduction in transition Reynolds number with reduction in unit Reynolds number as is commonly found in supersonic wind tunnels.

The total skin friction is roughly equal on upper and lower surfaces at zero incidence. With increase of incidence the value on the lower surface exceeds that on the upper but the total for both surfaces shows little change with incidence.

6. *Boundary Layer Development.*

The simple flat-plate estimates in Figs. 3 to 6 take no account of the effects of pressure gradients or of cross flows on the boundary-layer development. A full calculation could be made using the methods described by Cooke[10] but a complete description of the flow field round the wing would be a forbidding undertaking. A limited calculation was therefore made for the boundary-layer growth between two stations at different fore and aft positions on the wing with the wing at the design condition ($M = 2{\cdot}1$, $\alpha = 5{\cdot}3$ degrees). The stations $\frac{x}{c_0} = 0{\cdot}667$ and $\frac{x}{c_0} = 0{\cdot}8$ were chosen, as being in a region of adverse pressure gradient for most of the span of the wing upper surface. The procedure adopted was to assume a flat-plate relationship between skin-friction coefficient and momentum thickness at the upstream station, and by use of the momentum equation to derive the relationship at the downstream station. If the same skin friction-momentum thickness relationship is obtained then it can be concluded that the pressure gradients do not directly influence the skin friction locally and that the low values of skin friction measured result from pressure gradient and crossflow effects on the boundary-layer development.

Following Cooke[10] the momentum equation for a three-dimensional boundary layer with small crossflow becomes that for an analogous body of revolution of radius r,

$$\theta' + \theta \left\{ (H+2)\frac{u_1'}{u_1} + \frac{r'}{r} + \frac{\rho_1'}{\rho_1} \right\} = \frac{\tau}{\rho_1 u_1^2} \tag{1}$$

where primes denote differentiation with respect to ξ, the distance along a streamline. The term $\frac{r'}{r}$ is

determined by the convergence or divergence of the streamlines on the body. Approximately

$$\frac{r'}{r} = \frac{d\chi}{dy} \tag{2}$$

where χ is the angle which the surface streamlines make with some datum in the surface.

Expressing u_1 and ρ_1 in terms of M_1, the local Mach number outside the boundary layer, and assuming isentropic flow, equation (1) becomes

$$\theta' + \theta \left\{ \frac{d\chi}{dy} + \tfrac{1}{2} \frac{q_0}{q_1} \frac{dC_p}{d\xi} (M_1^2 - H - 2) \right\} = \frac{c_{f_1}}{2} \tag{3}$$

where c_{f_1} is the local skin-friction coefficient referred to local kinetic pressure q_1, and C_p is the pressure coefficient referred to freestream kinetic pressure q_0.

Using a value for the incompressible shape factor H of 1·35 as being appropriate for a flat-plate boundary layer at about the Reynolds number on the wing, with the compressibility correction of Spence[11], then for zero heat transfer and a recovery factor of 0·89, there is obtained

$$H = 1{\cdot}35\,(1 + 0{\cdot}31\,M_1^2). \tag{4}$$

Hence (3) becomes

$$\theta' + \theta \left\{ \frac{d\chi}{dy} + \frac{q_0}{q_1} (0{\cdot}29\,M_1^2 - 1{\cdot}68) \frac{dC_p}{d\xi} \right\} = \frac{c_{f_1}}{2}. \tag{5}$$

Using this equation at both stations on the wing and denoting values at the upstream station, $\frac{x}{c_0} = 0{\cdot}667$, by suffix A and at the downstream station, $\frac{x}{c_0} = 0{\cdot}8$, by suffix B then

$$\theta'_A + \theta_A F_A = \tfrac{1}{2} c_{f_{1A}} \tag{6}$$

and

$$\theta'_B + \theta_B F_B = \tfrac{1}{2} c_{f_{1B}} \tag{7}$$

where

$$F = \frac{d\chi}{dy} + \frac{q_0}{q_1} (0{\cdot}29\,M_1^2 - 1{\cdot}68) \frac{dC_p}{d\xi}. \tag{8}$$

Now approximately the change in momentum thickness between a point at station A and a point at B on the same streamline will be given by

$$\theta_B - \theta_A = \tfrac{1}{2} (\theta'_A + \theta'_B)(\xi_B - \xi_A). \tag{9}$$

Eliminating θ'_A and θ'_B from equations (6), (7), (9) an expression for θ_B is obtained

$$\theta_B = \frac{\theta_A + \frac{1}{2}(\xi_B - \xi_A) \left\{ \frac{1}{2} (c_{f_{1A}} + c_{f_{1B}}) - \theta_A F_A \right\}}{1 + \frac{1}{2} F_B (\xi_B - \xi_A)}. \tag{10}$$

In this equation measured values of c_{f_1} were used and θ_A was obtained from $c_{f_{1A}}$ assuming a flat plate relationship. The position of points at A and B on the same streamline was obtained by assuming that the mean direction of the external streamlines between the two stations is given by the mean of the values at the two stations.

The direction of the external streamlines is not easy to define or measure since it varies with distance normal to the surface, and the value required is that at the edge of the boundary layer. The value actually used was defined in the following way. At each of the two stations the flow directions relative to the model were measured at points on a series of circular arcs described about the model centreline. The results are shown in Figs. 13 and 14. For each circular arc a pair of axes was defined as the tangent and normal to the section shape in the plane of the flow survey at the point of intersection of the arc with the section. The flow directions referred to these axes were plotted against distance from the surface, giving a roughly linear variation which was extrapolated to give the directions at the surface. These are, of course, fictitious directions and not the actual flow directions at the surface within the boundary layer, the surface being used only to define a boundary more clearly than 'the edge of the boundary layer'. The flow directions derived this way are shown in Figs. 15 and 16. The angle shown in Fig. 15 is a close approximation to χ defined in equation (2). χ is an angle in a plane tangent to the surface at a given point, whereas the angle in Fig. 15 is in a plane tangent to the wing cross section but parallel to the wing centreline. The direction is measured with respect to that of the wing centreline. The angles in Fig. 16 are shown largely for interest but do give some confidence in the procedure in that they are in fair agreement with the wing surface slope $\left(\frac{\partial z}{\partial x}\right)$ evaluated along lines of constant span. From Fig. 15 the streamline divergence was calculated and the smoothed results are shown in Fig. 17. A positive value of $\frac{d\chi}{d(\frac{y}{s})}$ means a divergence of the flow and a negative value a convergence.

From the flow directions the spanwise co-ordinates of points on the upstream and downstream stations on the same streamline was calculated and their relationship is shown in Fig. 18 for both surfaces.

The pressure gradients in the direction of the streamlines obtained by numerical differentiation of the measured pressure coefficients are given in Fig. 19.

The local Mach number and also the local kinetic pressure to be used in equation (8) were calculated from the pressure coefficient at each point assuming isentropic flow. The local Mach number could also be derived from the flow survey. For interest the two values are compared in Fig. 20. Agreement is fairly good except for the upper surface for $\frac{x}{c_0} = 0{\cdot}8$. The values obtained from the pressure coefficients, and the corresponding kinetic pressure assuming isentropic flow, were used in equation (10).

To obtain momentum thickness the local and average skin-friction logarithmic formulae as given by Wieghardt and Prandtl-Schlichting were combined. Compressibility was taken into account following Spence[11]. He showed that by applying the intermediate enthalpy concept to an incompressible skin-friction relationship of the form

$$c_f = f(Re_\theta)$$

a compressible form results,

$$\frac{\rho_1}{\rho^*} c_f = f\left(\frac{\mu_1}{\mu^*} Re_\theta\right)$$

where Re_θ is a momentum-thickness Reynolds number based on conditions outside the boundary layer, ρ_1, μ_1 are density and viscosity outside the boundary layer and ρ^*, μ^* are intermediate enthalpy values. The numerical values used are those given in Ref. 8 and plotted in Fig. 21 as the full line. Assuming this relationship holds at the upstream station A the corresponding relationships at station B, for upper and lower surfaces were calculated, using equation (10) for θ. The result is shown in Fig. 21 where the measured skin-friction coefficient c_{f_1} is plotted against Re_θ with appropriate compressibility corrections. It will be seen that on the lower surface where there are mainly favourable gradients the derived relationship agrees with the original assumption to within about 10 per cent. On the upper surface, however,

the discrepancy is up to about 30 per cent suggesting that even the very mild adverse pressure gradient there has a strong effect on the local skin friction. In fact the inclusion of the pressure gradient and flow convergence terms in the momentum equation has only a very small effect on the calculated curves. If these terms are omitted the change in calculated Re_θ is less than 10 per cent, giving slightly less discrepancy for the lower surface and slightly more for the upper surface. The mechanism of the discrepancy has not been pursued further on this model because of the experimental complexity. Instead, an attempt has been made to obtain an axial analogue of the same type of flow on a body of revolution. By using a body with a waist followed by a flare, regions with favourable and unfavourable pressure gradients with converging and diverging flows of the same order of magnitude as on the wing have been obtained. The skin friction in the waist of the body has been found to be low as in the adverse pressure gradient on the wing upper surface. This experiment is described in Refs. 2 and 3 where it is shown that the combined effect of adverse pressure gradient and streamline convergence results in boundary-layer profiles with a large wake component and low skin-friction coefficient.

7. *Conclusions.*

The local skin friction measured on the wing by the razor blade technique shows large effects of pressure gradient and streamline convergence or divergence. Application of the boundary-layer momentum equation to the measurements suggests that the effects arise as a direct consequence of modification of the boundary-layer profile and hence the skin friction, the terms in the momentum equation from the pressure gradient and streamline direction being far too small to explain the results. Despite the wide variations in skin friction on the wing surface the total skin-friction drag is probably only some 5 to 10 per cent less than that on a flat plate. The drag shows little variation with incidence; a decrease on the upper surface approximately compensates an increase on the lower surface.

Further explanation of the skin-friction behaviour is being sought using a body of revolution with a flow analogous to that on the wing.

Acknowledgement.

The authors would like to acknowledge help from Mr. A. O. Ormerod who made available to them his measurements of the forces and pressure distribution on the model.

LIST OF SYMBOLS

c_0	Wing-root chord
c_f	Local skin-friction coefficient based on freestream conditions
C_p	Pressure coefficient based on freestream conditions
$-C_X$	Axial-force coefficient based on plan area
$-C_{X_T}$	Skin-friction axial-force coefficient from total measured force minus integrated pressure force
$-C_{X_F}$	Skin-friction axial-force coefficient from integration of measured skin friction
F	*See* equation (8)
H	Boundary-layer shape parameter
M	Mach number
q	Kinetic pressure
r	Radius of analogous body of revolution
s	Wing local semi-span
s_0	Wing maximum semi-span
Re_θ	Reynolds number based on momentum thickness
Re_{c_0}	Reynolds number based on root chord
u	Velocity
x	Longitudinal co-ordinate measured from nose
y	Spanwise co-ordinate measured from root
z	Co-ordinate normal to x, y
α	Incidence
χ	Streamline direction measured relative to the model root-chord direction in a plane tangential to wing sections normal to root chord; outflow positive
θ	Momentum thickness
ρ	Density
τ	Surface shearing stress
ξ	Distance along streamline

Subscripts

0	Freestream
1	Local outside boundary layer
A	Station $x = 40$ in.
B	Station $x = 48$ in.

Superscript* refers to intermediate enthalpy conditions.

Primes denote differentiation with respect to ξ.

REFERENCES

No.	*Author(s)*	*Title, etc.*
1	K. G. Smith, L. Gaudet and K. G. Winter ..	The use of surface pitot tubes as skin-friction meters at supersonic speeds. ARC, R & M 3351, June 1962.
2	K. G. Winter, K. G. Smith and J. C. Rotta	Turbulent boundary-layer studies on a waisted body of revolution in subsonic and supersonic flow. AGARDograph 97, Part II, pp. 933–961. May 1965.
3	K. G. Winter, J. C. Rotta .. and K. G. Smith	Untersuchungen der turbulenten Grenzschicht an einem taillierten Drehkörper bei Unterund Überschallströmung. DLR FB 65–52, November 1965.
4	G. M. Roper	Use of camber and twist to produce low-drag delta or sweptback wings, without leading-edge singularities, at supersonic speeds. A.R.C. R & M 3196. December 1958.
5	L. Gaudet and K. G. Winter	Preliminary measurements of the flow field on the leeside of a delta wing of unit aspect ratio at a Mach number of 2·6 and an incidence of 15 deg. R.A.E. T.N. No. Aero 2787, September 1961 A.R.C. 23 510.
6	F. J. Centolanzi	Characteristics of a 40 deg. cone for measuring Mach number, total pressure and flow angles at supersonic speeds. NACA T.N. 3967, May 1957.
7	J. C. Cooke	Boundary-layer flow between the attachment lines on a flat plate delta wing at incidence. Aero Quart Vol. 13, pp. 1 to 16, 1962.
8	K. G. Smith	Methods and charts for estimating skin-friction drag in wind-tunnel tests with zero heat transfer. A.R.C. C.P. 824, August 1964.
9	J. Y. G. Evans	Transition fixing techniques and the interpretation of boundary layer conditions on slender wings in supersonic wind tunnels. R.A.E. T.N. No. Aero 2946, February 1964, A.R.C. 25 892.
10	J. C. Cooke	An axially symmetric analogue for general three dimensional boundary layers. A.R.C. R & M 3200. June 1959.
11	D. A. Spence	The growth of compressible turbulent boundary layers on isothermal and adiabatic walls. A.R.C. R & M 3191, June 1959.

APPENDIX

Equations to wing surface

For the wing upper surface

$$z_u = z_c + z_t$$

and for the lower surface

$$z_l = z_c - z_t$$

where z_c is the camber and z_t the thickness

The camber surface is given by

$$\frac{z_c}{c_0} = 0{\cdot}09244963\left(\frac{x}{c_0}\right) - 0{\cdot}94305757\left(\frac{x}{c_0}\right)^3 + 1{\cdot}56722639\left(\frac{x}{c_0}\right)^4 - 0{\cdot}71661845\left(\frac{x}{c_0}\right)^5 +$$

$$+\left(\frac{y}{c_0}\right)^2 \left\{-10{\cdot}41953298 + 32{\cdot}21463018\left(\frac{x}{c_0}\right) - 33{\cdot}75316994\left(\frac{x}{c_0}\right)^2 +\right.$$

$$\left. + 11{\cdot}95807274\left(\frac{x}{c_0}\right)^3\right\} +$$

$$+\left(\frac{y}{c_0}\right)^4 \left\{-13{\cdot}009573 + 13{\cdot}009573\left(\frac{x}{c_0}\right)\right\}$$

and the thickness by

$$\frac{z_t}{c_0} = 0{\cdot}07875\left\{\frac{x}{c_0} - 3\frac{y}{c_0}\right\}\left\{1 - \frac{x}{c_0}\right\}\left\{4 - 6\frac{x}{c_0} + 4\left(\frac{x}{c_0}\right)^2 - \left(\frac{x}{c_0}\right)^3\right\}.$$

Outboard of the line joining the leading edge at $\frac{y}{c_0} = 0{\cdot}2672$ and the trailing edge at $\frac{y}{c_0} = 0{\cdot}1083$ the thickness distribution was modified to be conical with respect to the tip.

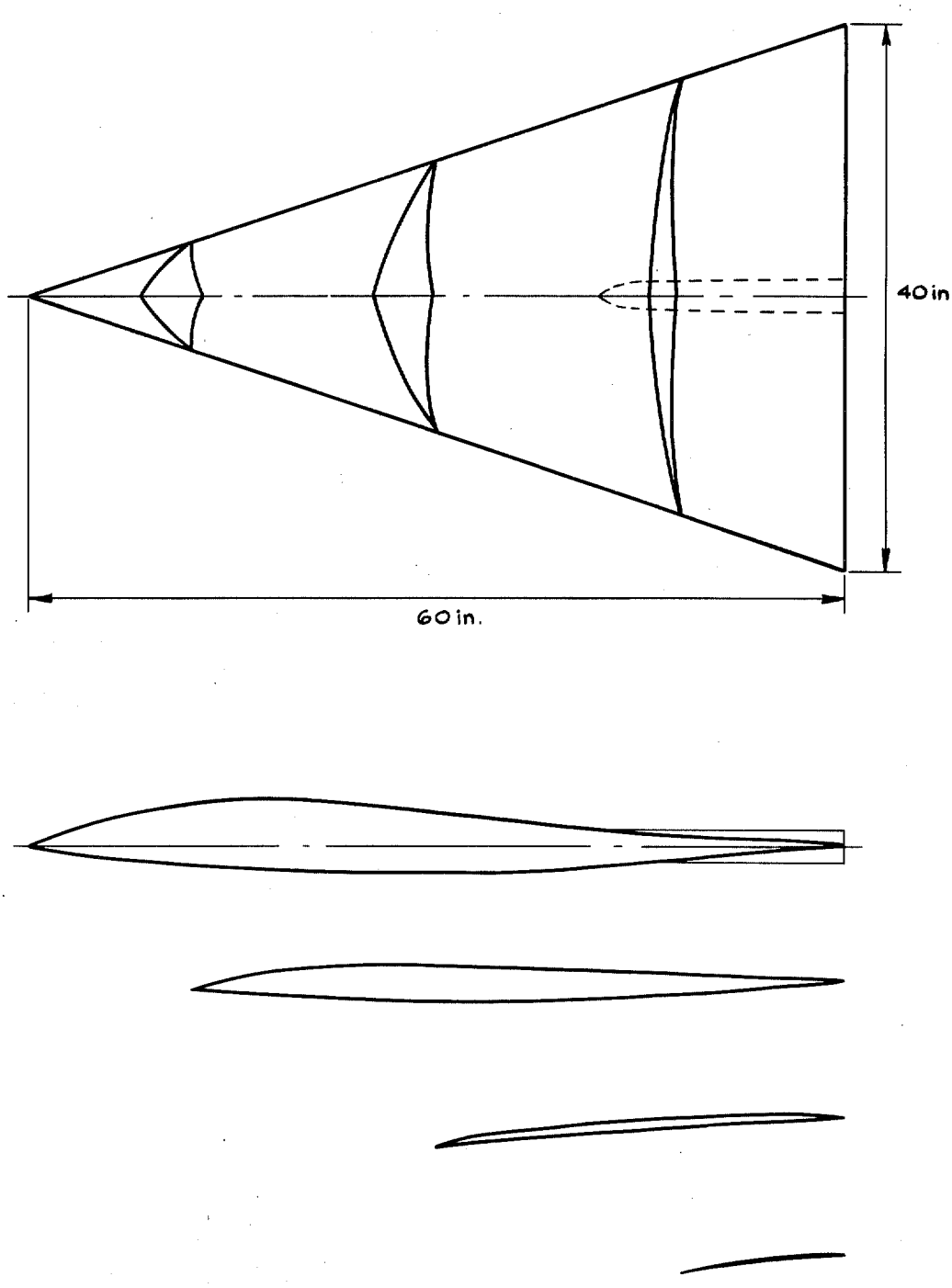

FIG. 1. General arrangement of model.

FIG. 2. Model mounted in 8 ft × 8 ft wind tunnel.

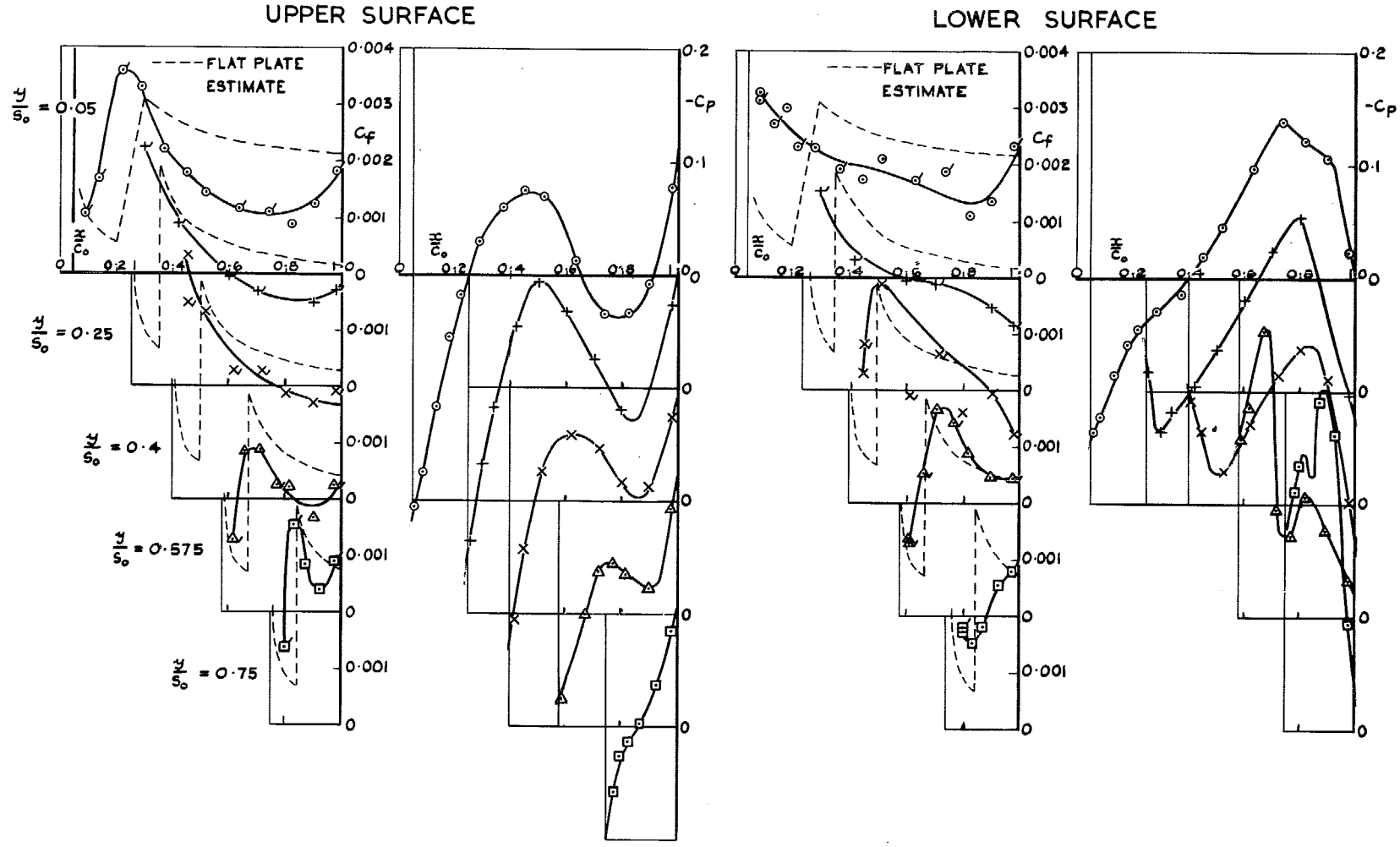

(a) $\alpha = 0$

FIG. 3. Skin friction and pressure coefficients $M = 1{\cdot}5$ $Re_{c_0} = 10^7$.

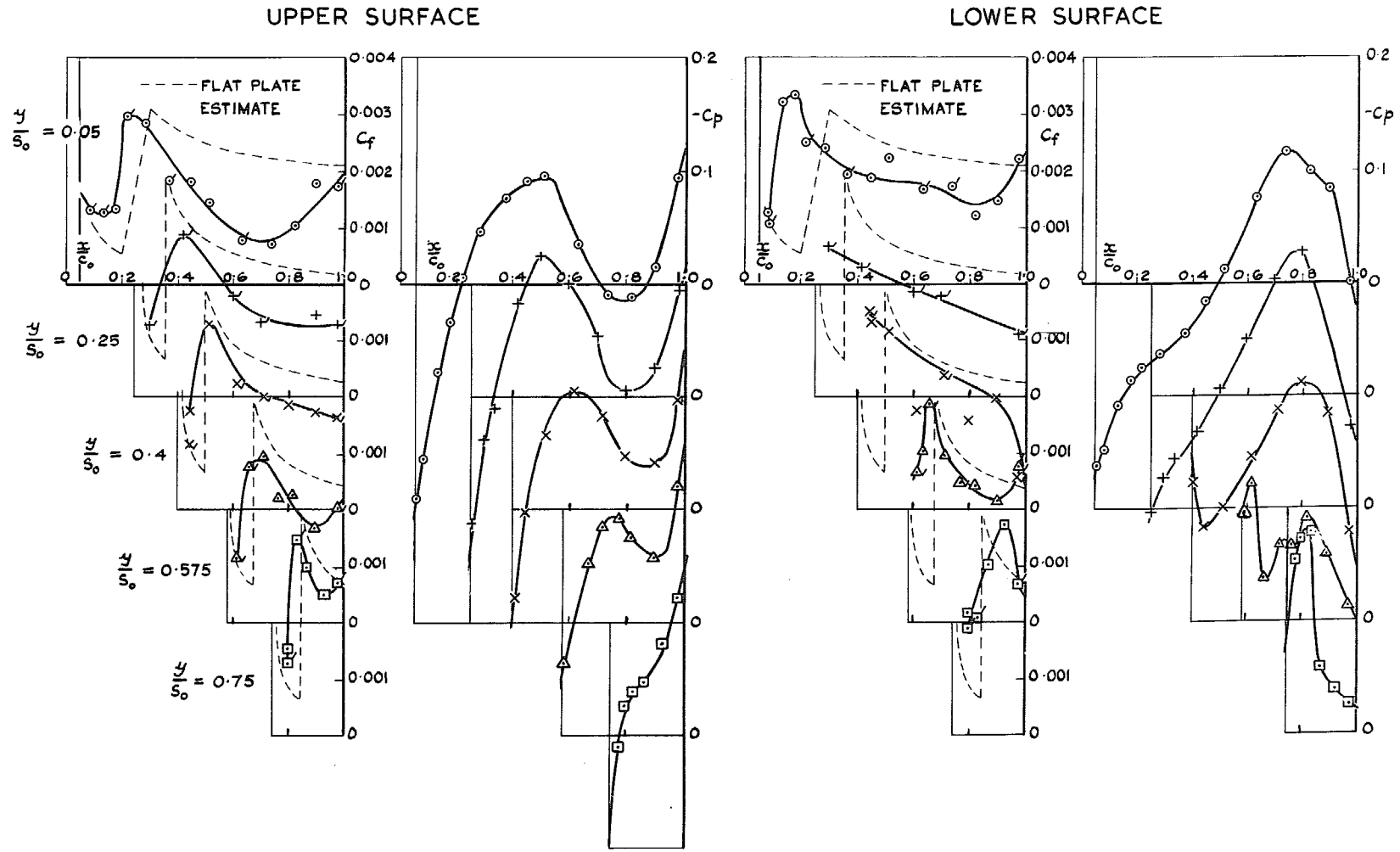

(b) $\alpha = 2°$

FIG. 3 (contd.). Skin friction and pressure coefficients $M = 1{\cdot}5$ $Re_{c_0} = 10^7$.

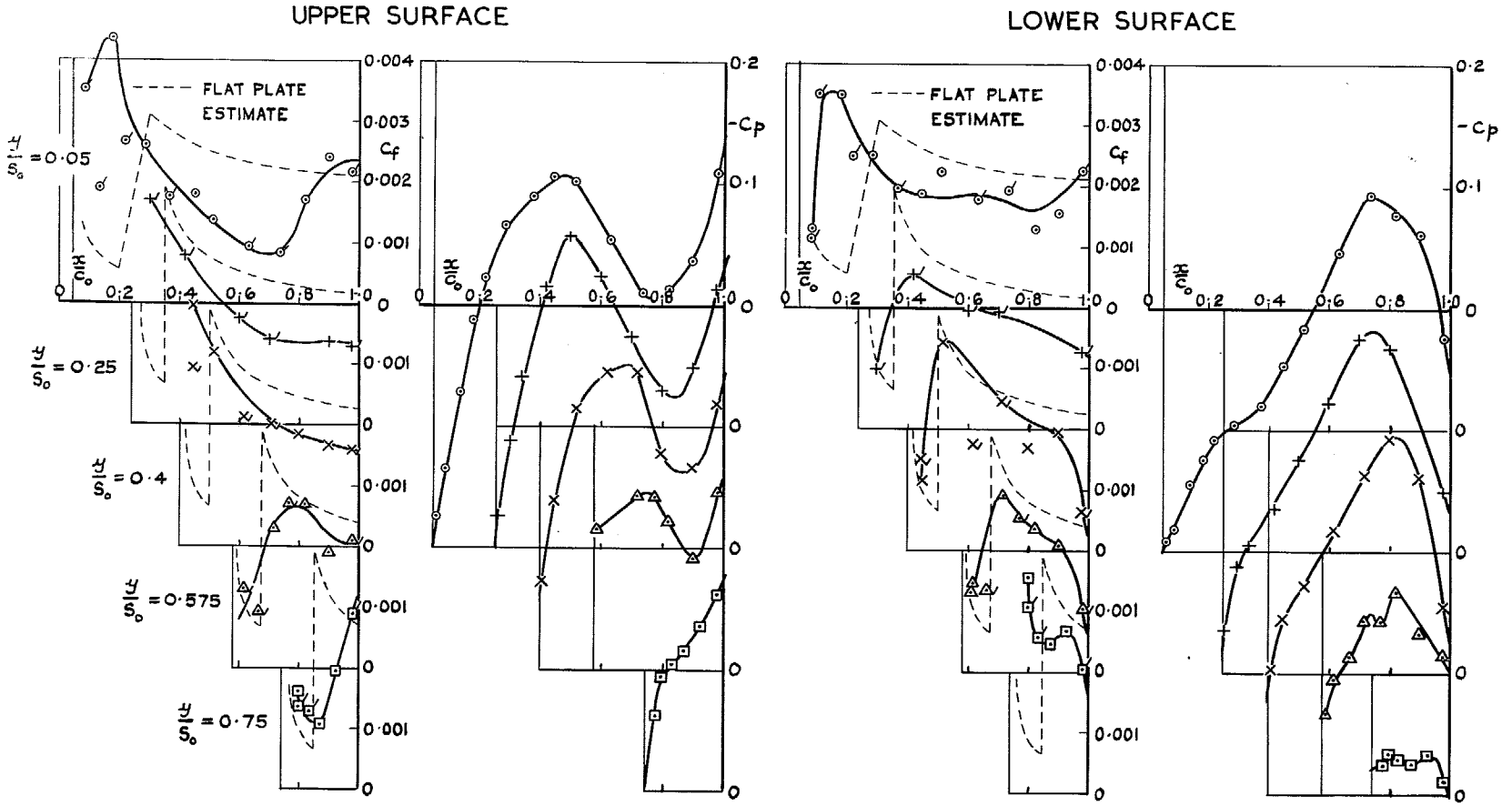

(c) $\alpha = 4°$

FIG. 3 (contd.). Skin friction and pressure coefficients $M = 1{\cdot}5$ $Re_{c_0} = 10^7$.

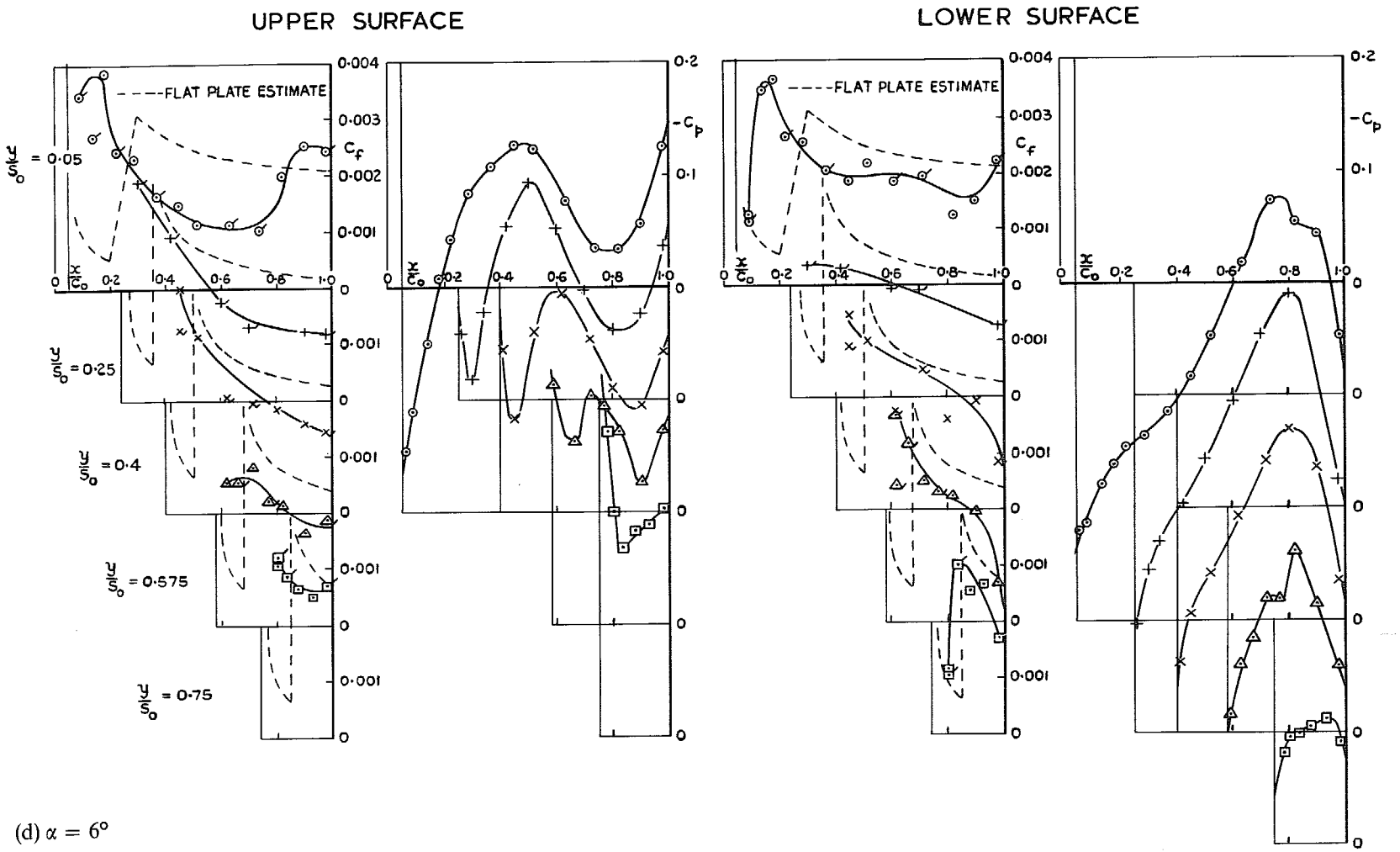

(d) $\alpha = 6°$

FIG. 3 (concl.). Skin friction and pressure coefficients $M = 1{\cdot}5$ $Re_{c_0} = 10^7$.

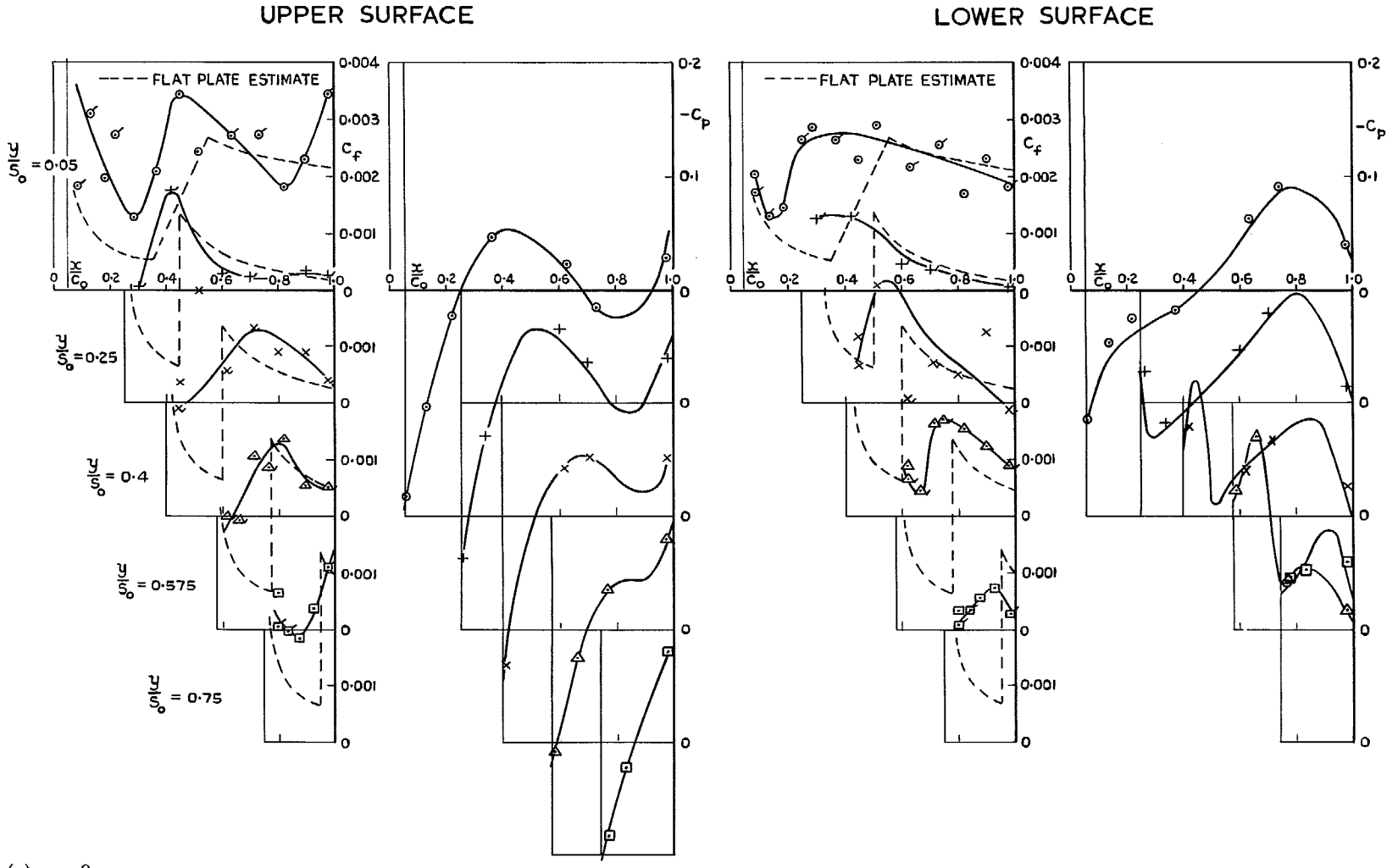

(a) $\alpha = 0$

FIG. 4. Skin friction and pressure coefficients $M = 2{\cdot}1$ $Re_{c_0} = 5 \times 10^6$.

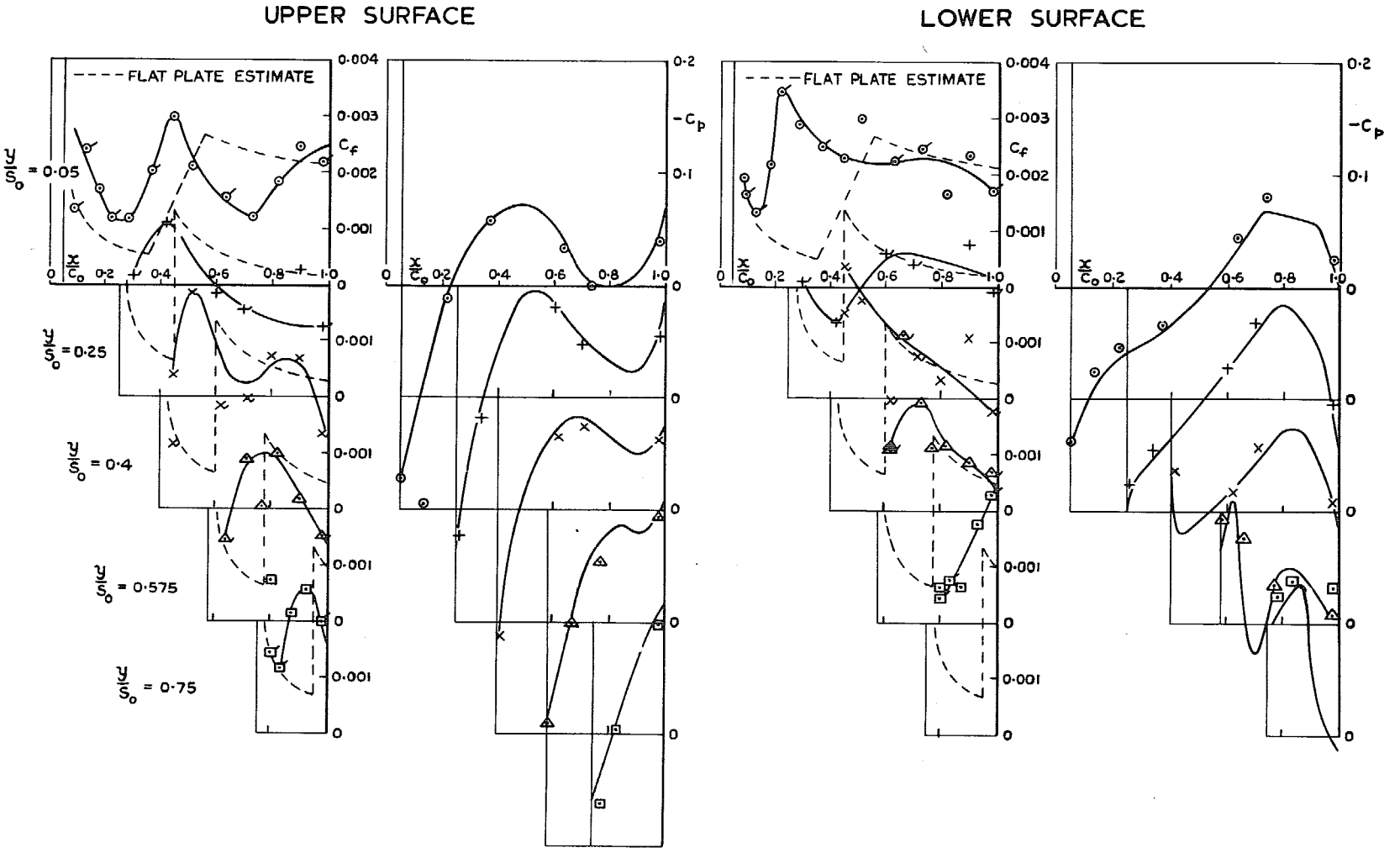

(b) $\alpha = 2°$

FIG. 4 (contd.). Skin friction and pressure coefficients $M = 2{\cdot}1$ $Re_{c_0} = 5 \times 10^6$.

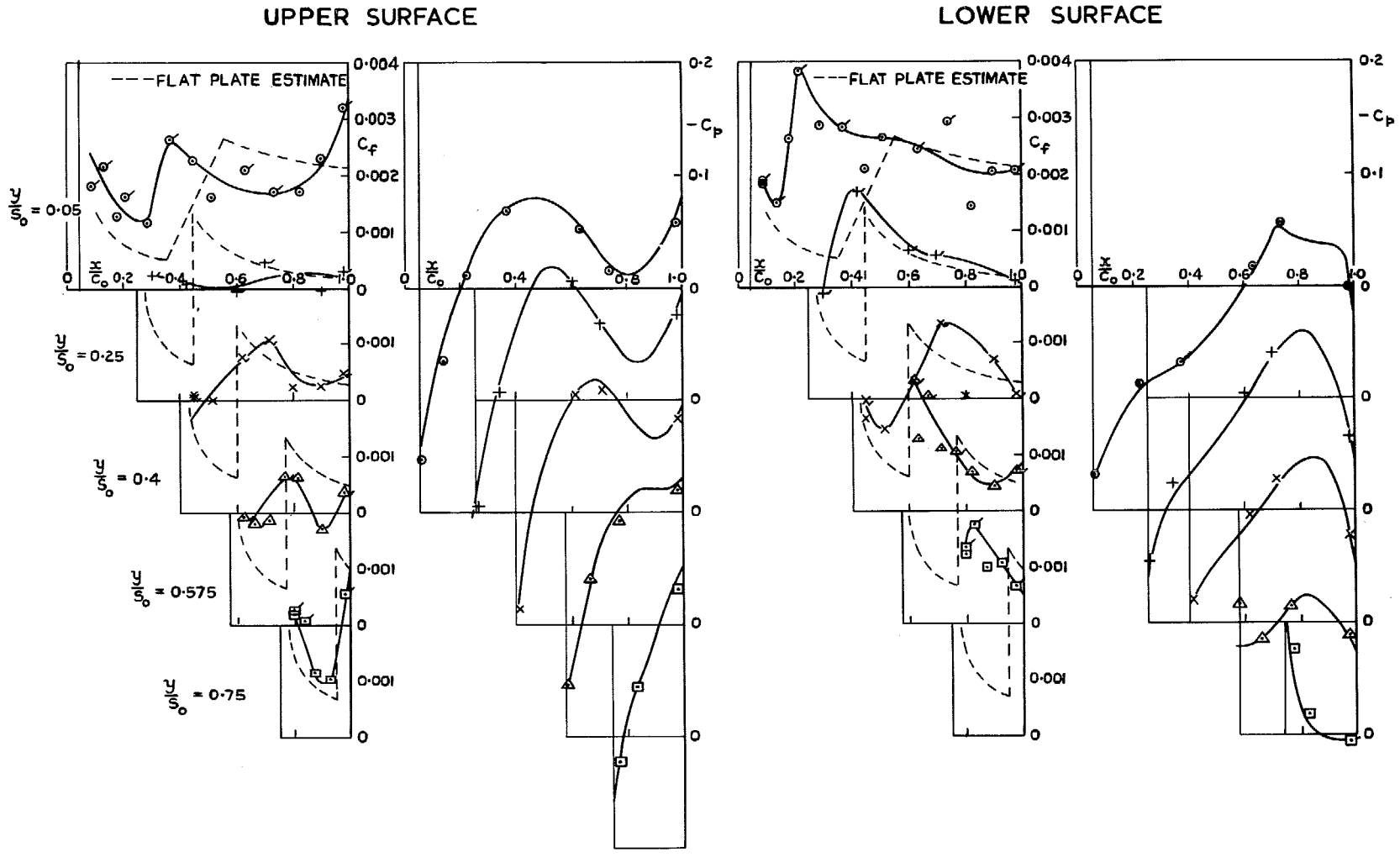

(c) $\alpha = 4°$

FIG. 4 (contd.). Skin friction and pressure coefficients $M = 2{\cdot}1$ $Re_{c_0} = 5 \times 10^6$.

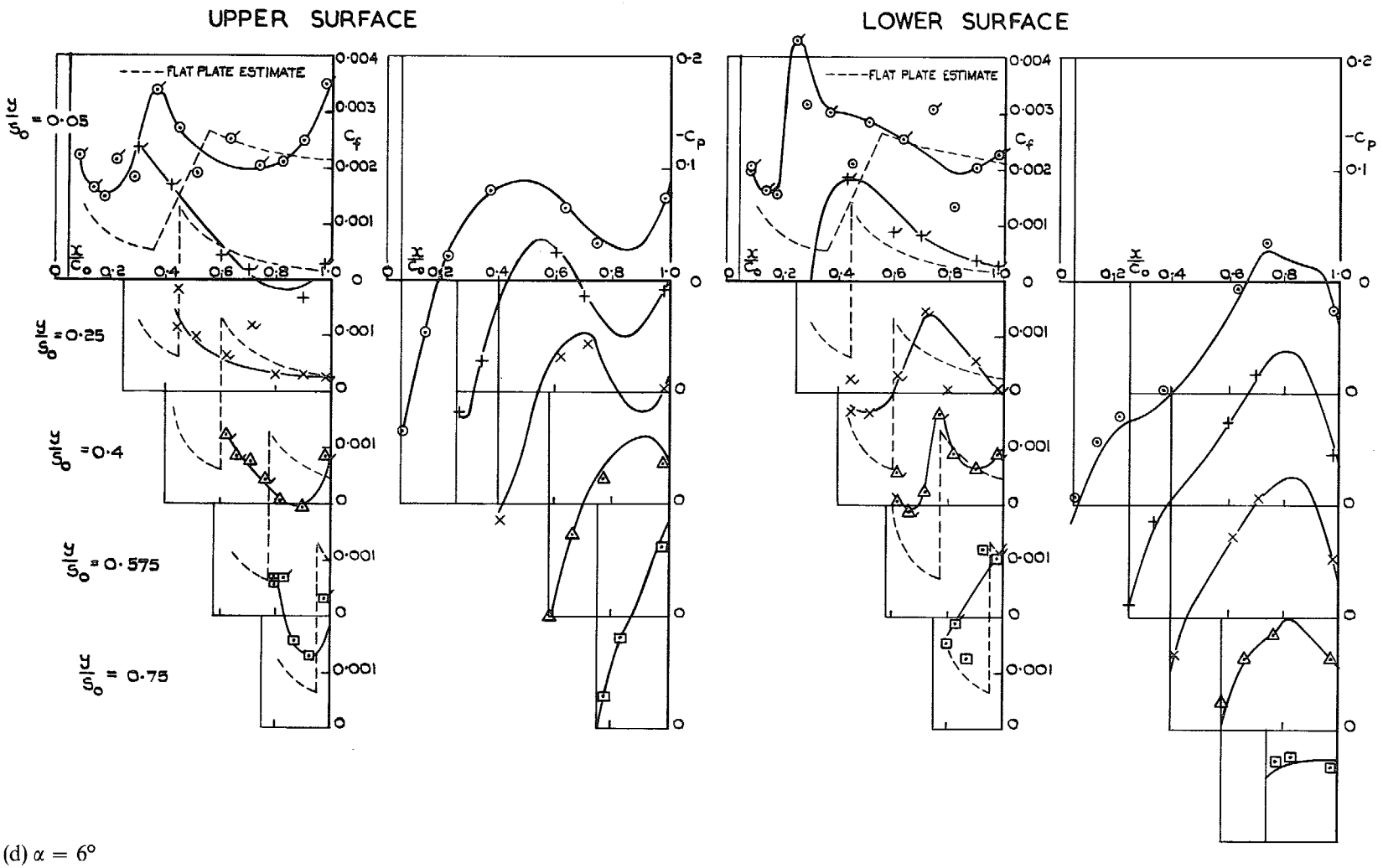

(d) $\alpha = 6°$

FIG. 4 (contd.). Skin friction and pressure coefficients $M = 2{\cdot}1$ $Re_{c_0} = 5 \times 10^6$.

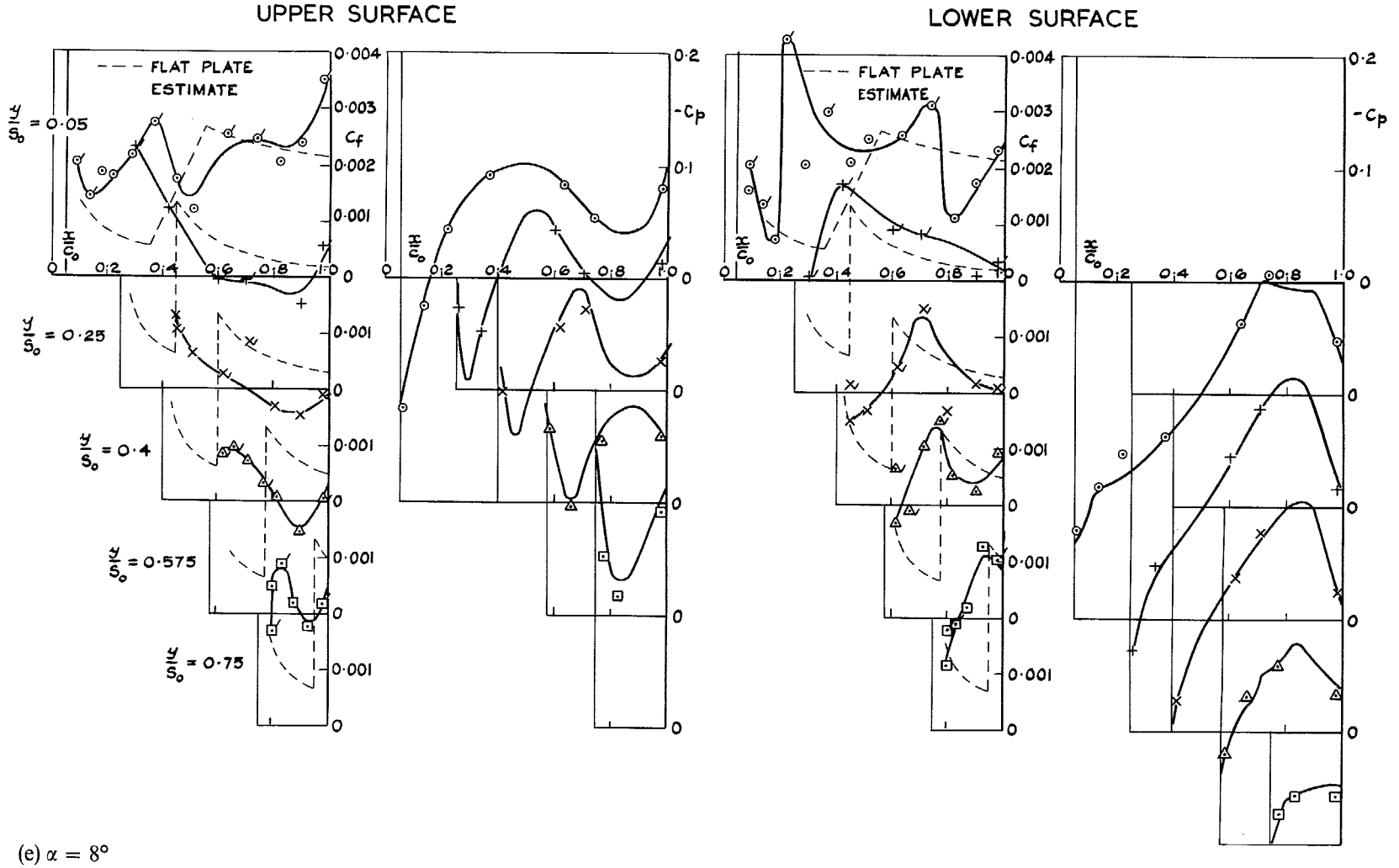

(e) $\alpha = 8°$

FIG. 4 (contd.). Skin friction and pressure coefficients $M = 2{\cdot}1$ $Re_{c_0} = 5 \times 10^6$.

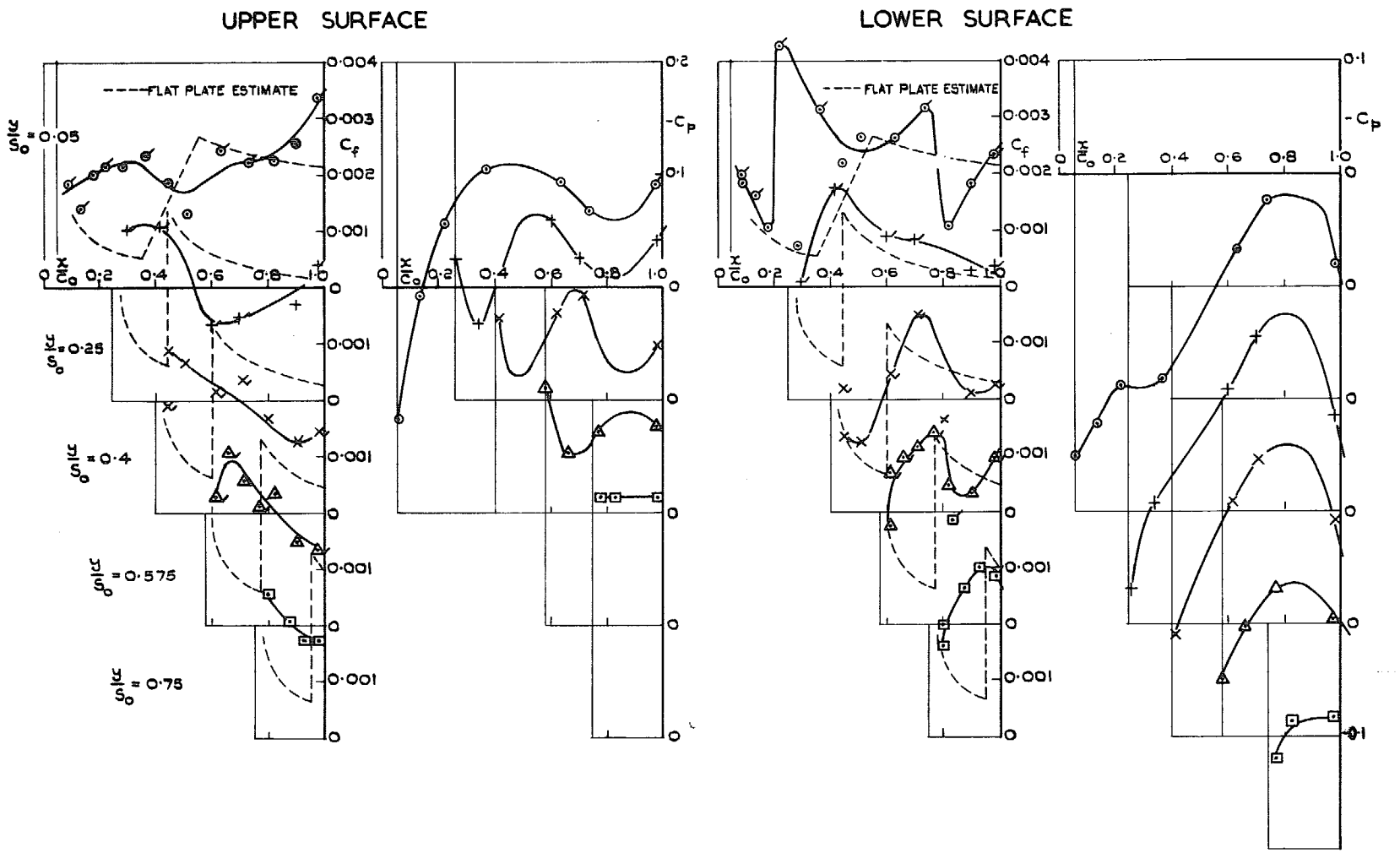

(f) $\alpha = 10°$

FIG. 4 (concl.). Skin friction and pressure coefficients $M = 2{\cdot}1$ $Re_{c_0} = 5 \times 10^6$.

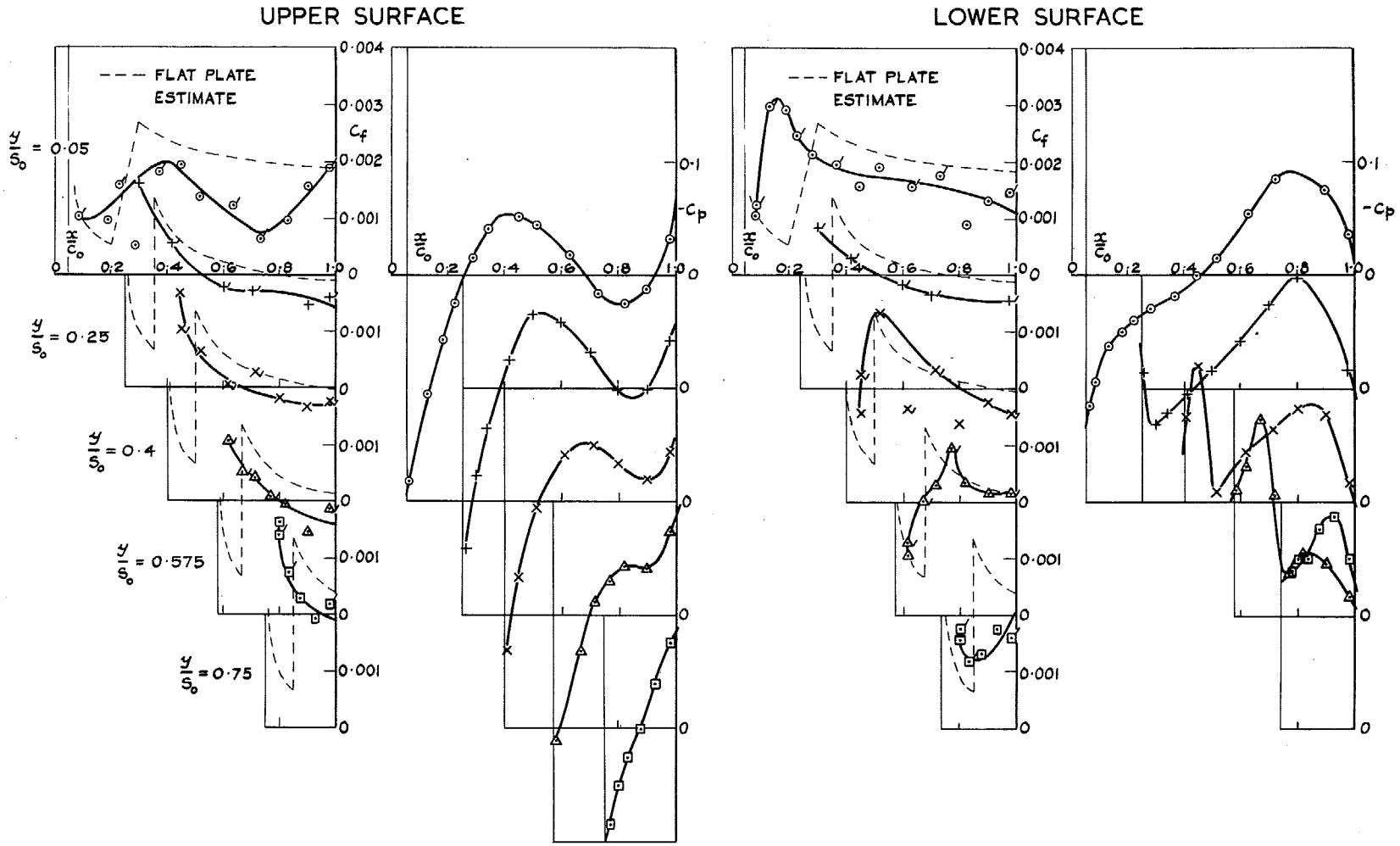

(a) $\alpha = 0$

FIG. 5. Skin friction and pressure coefficients $M = 2{\cdot}1$ $Re_{c_0} = 10^7$.

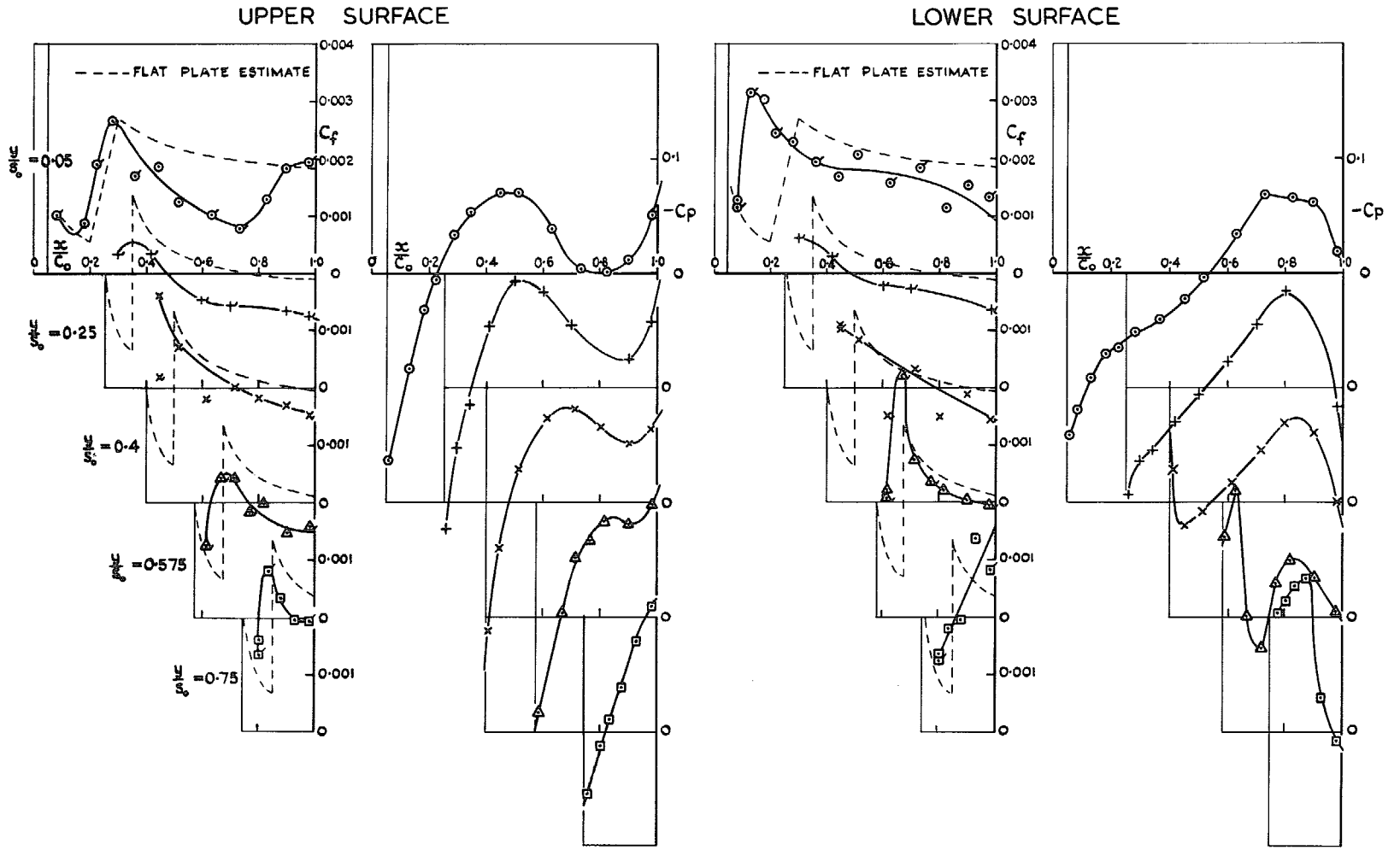

(b) $\alpha = 2°$

FIG. 5 (contd.). Skin friction and pressure coefficients $M = 2{\cdot}1$ $Re_{c_0} = 10^7$.

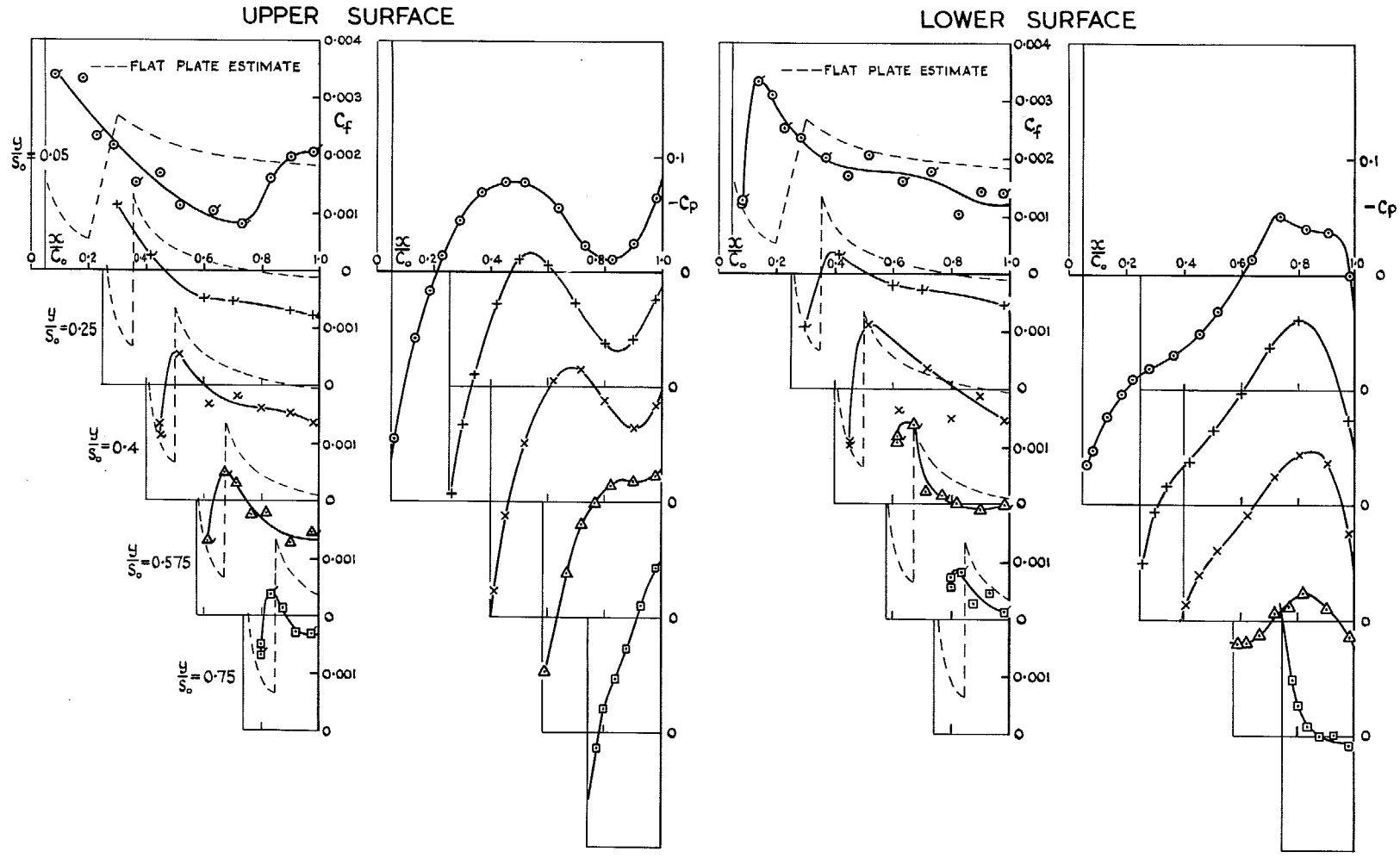

(c) $\alpha = 4°$

FIG. 5 (contd.). Skin friction and pressure coefficients $M = 2{\cdot}1$ $Re_{c_0} = 10^7$.

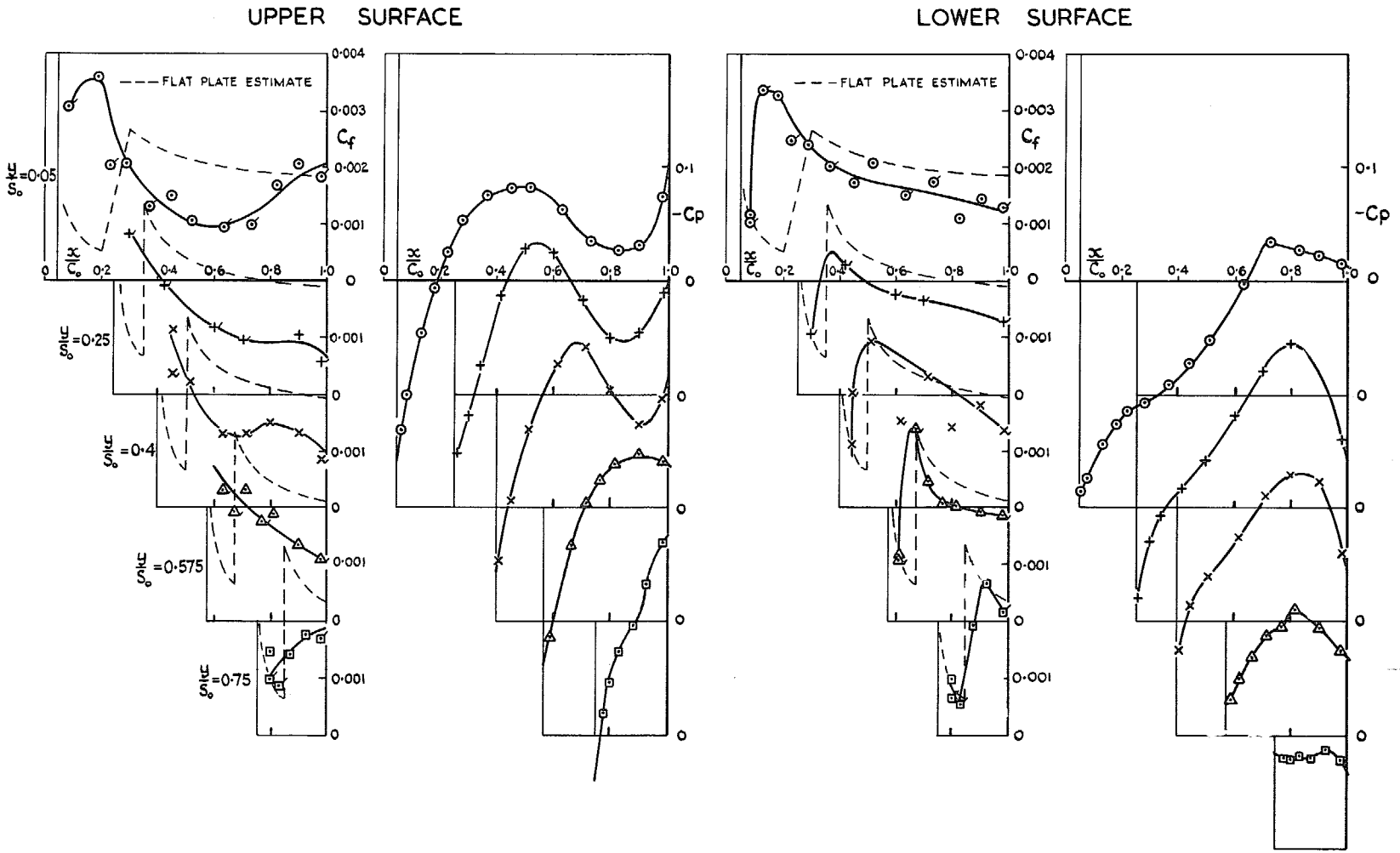

(d) $\alpha = 5{\cdot}3°$

FIG. 5 (contd.). Skin friction and pressure coefficients $M = 2{\cdot}1$ $Re_{c_0} = 10^7$.

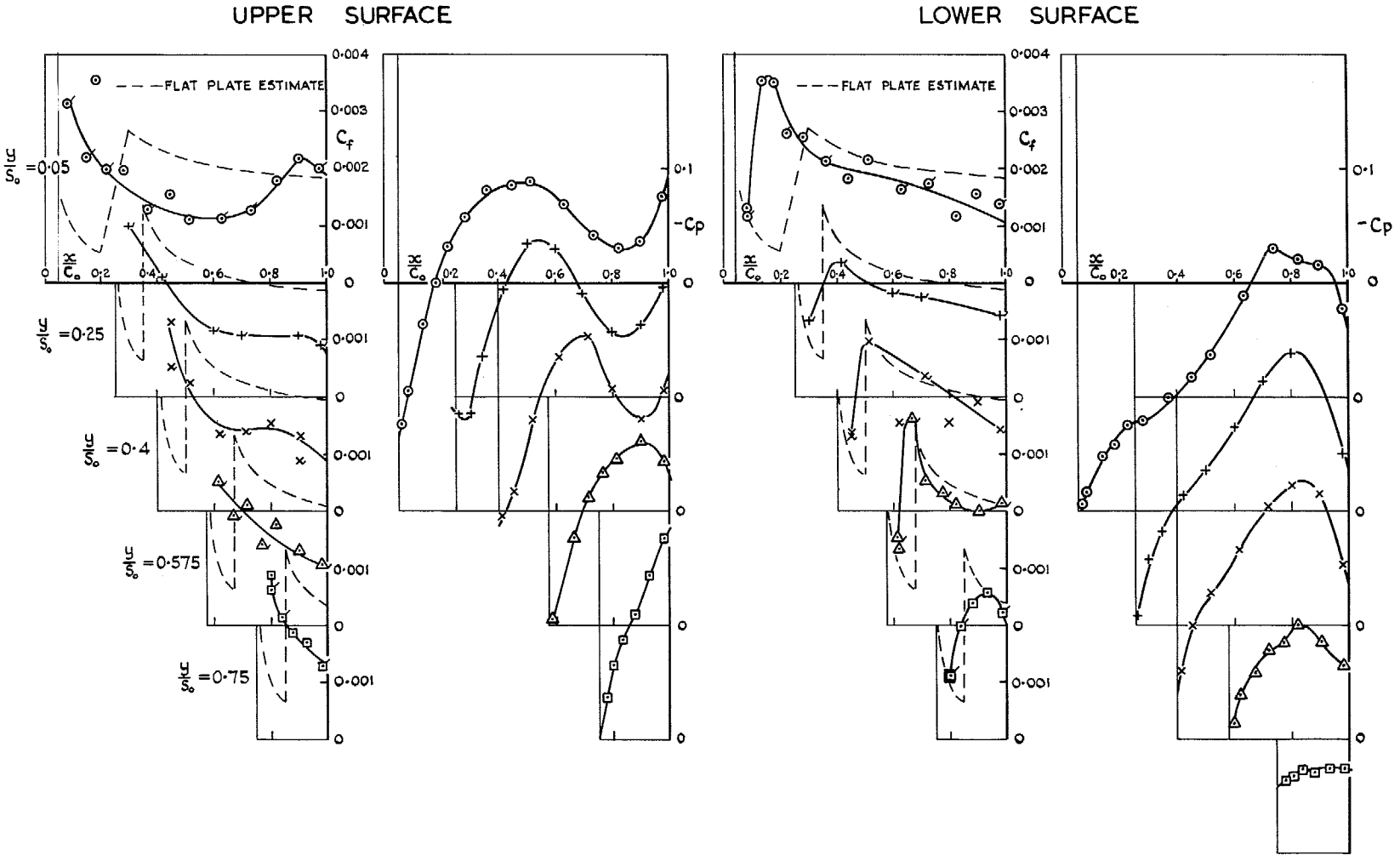

(e) $\alpha = 6°$

FIG. 5 (contd.). Skin friction and pressure coefficients $M = 2{\cdot}1$ $Re_{c_0} = 10^7$.

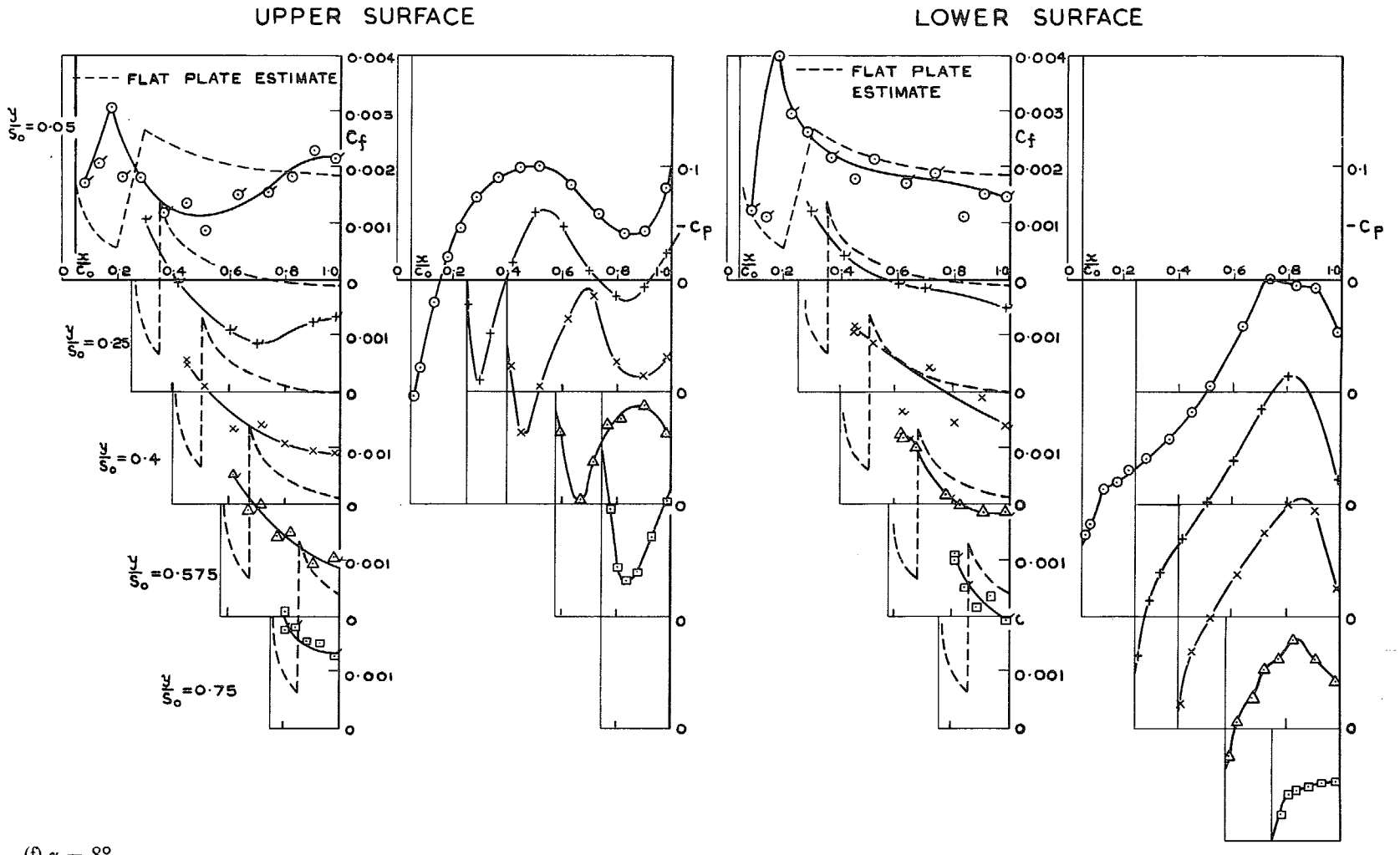

(f) $\alpha = 8°$

FIG. 5 (concl.). Skin friction and pressure coefficients $M = 2{\cdot}1$ $Re_{c_0} = 10^7$.

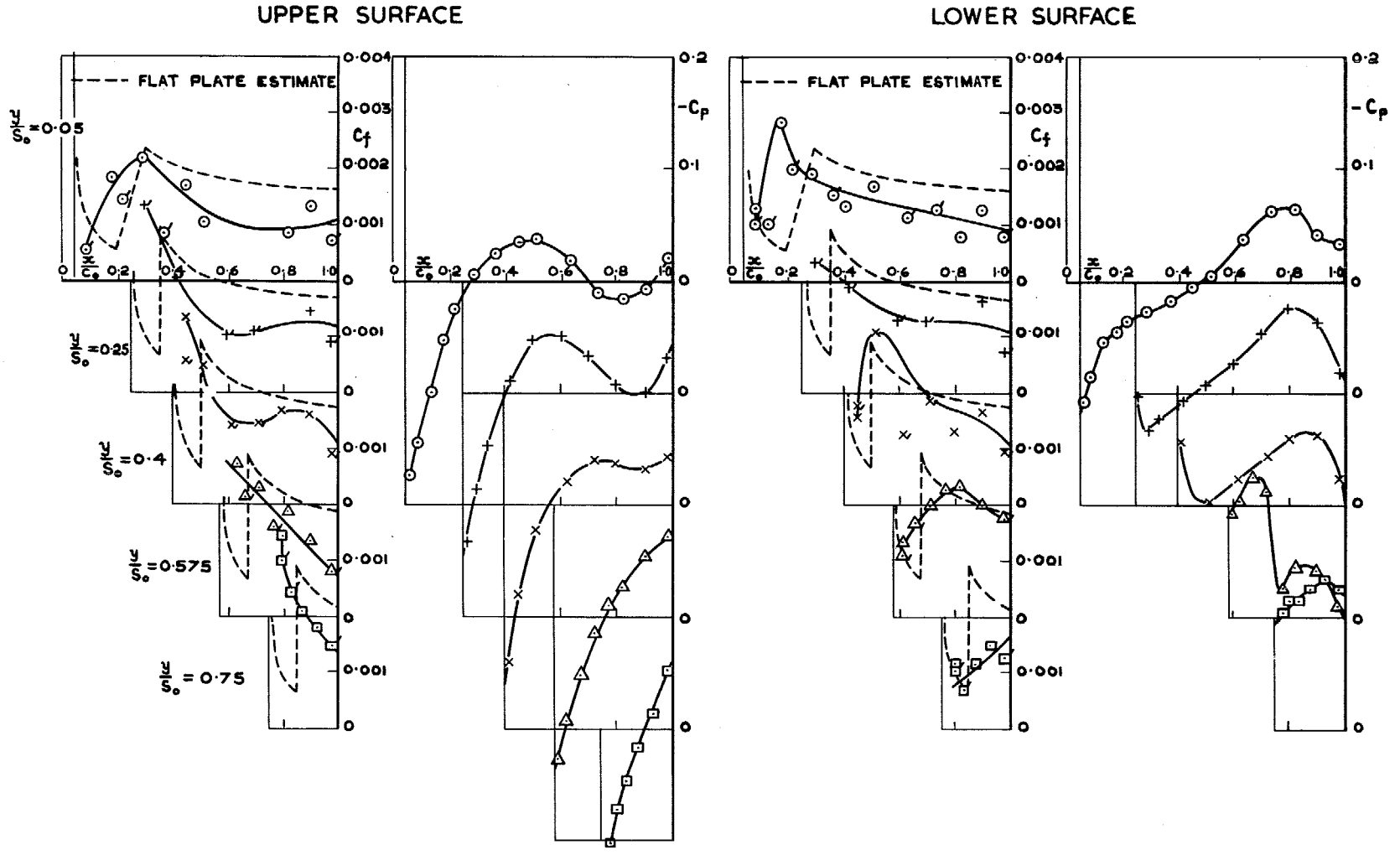

(a) $\alpha = 0$

FIG. 6. Skin friction and pressure coefficients $M = 2{\cdot}6$ $Re_{c_0} = 10^7$.

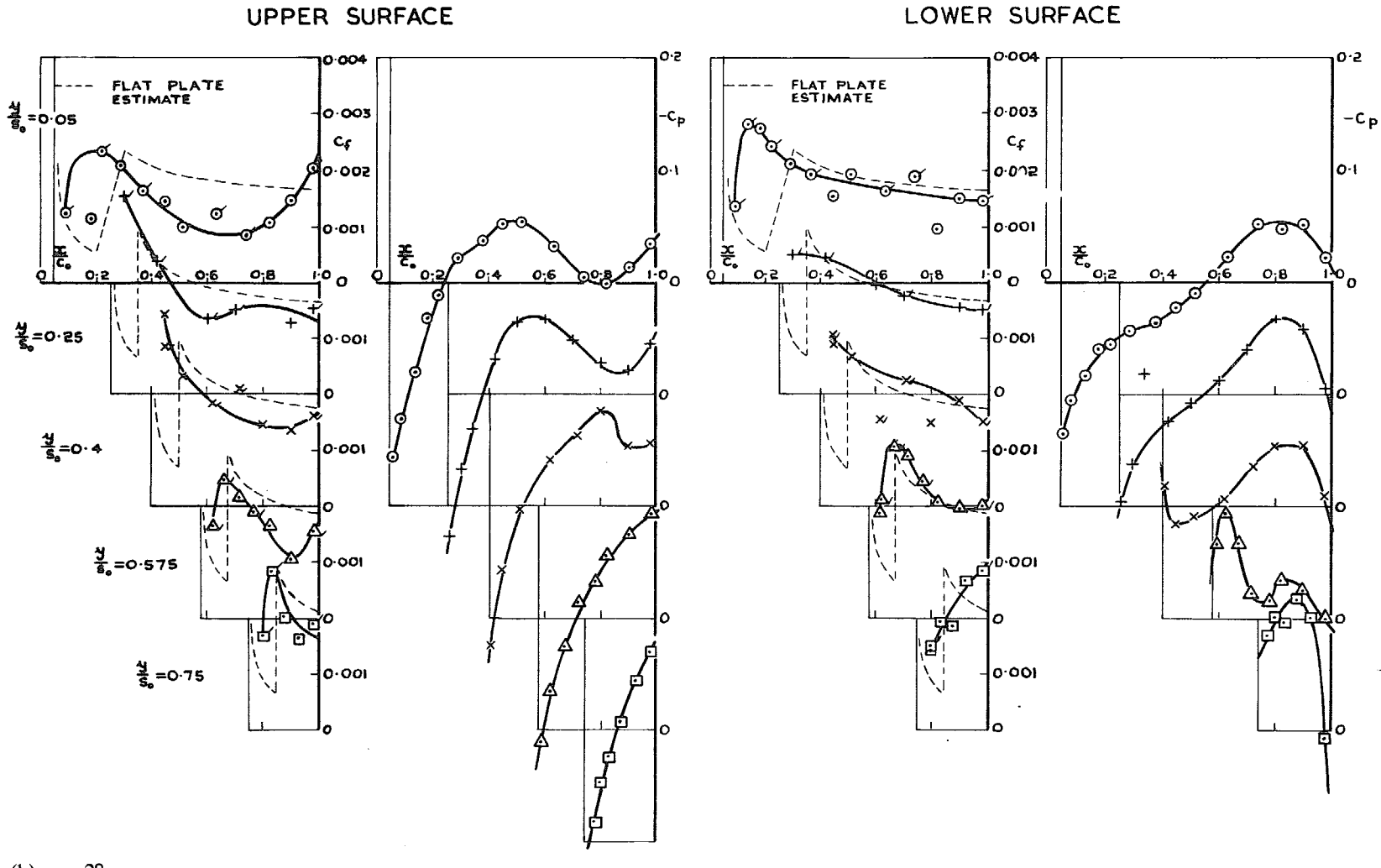

(b) $\alpha = 2°$

FIG. 6 (contd.). Skin friction and pressure coefficients $M = 2{\cdot}6$ $Re_{c_0} = 10^7$.

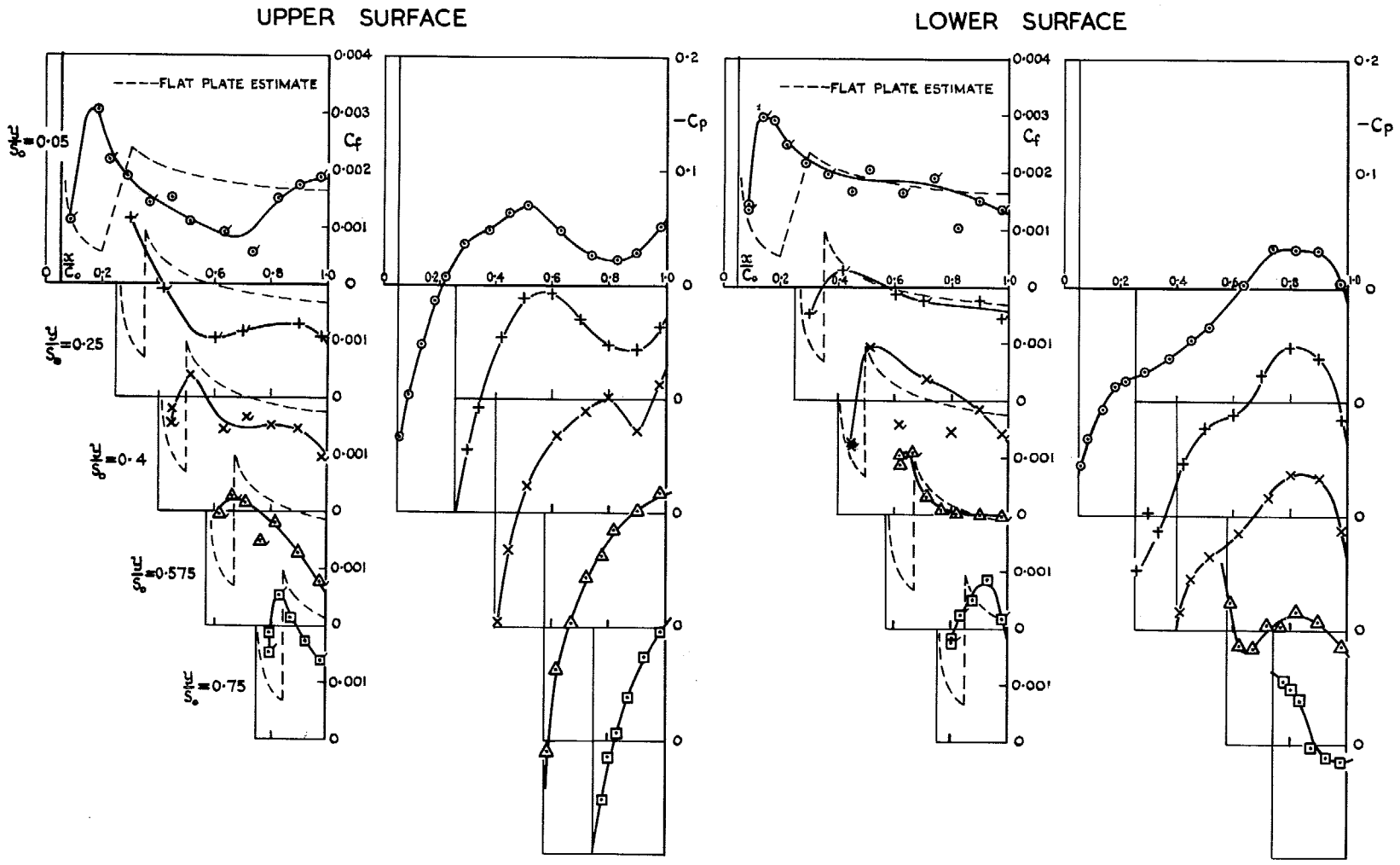

(c) $\alpha = 4°$

FIG. 6 (contd.). Skin friction and pressure coefficients $M = 2{\cdot}6$ $Re_{c_0} = 10^7$.

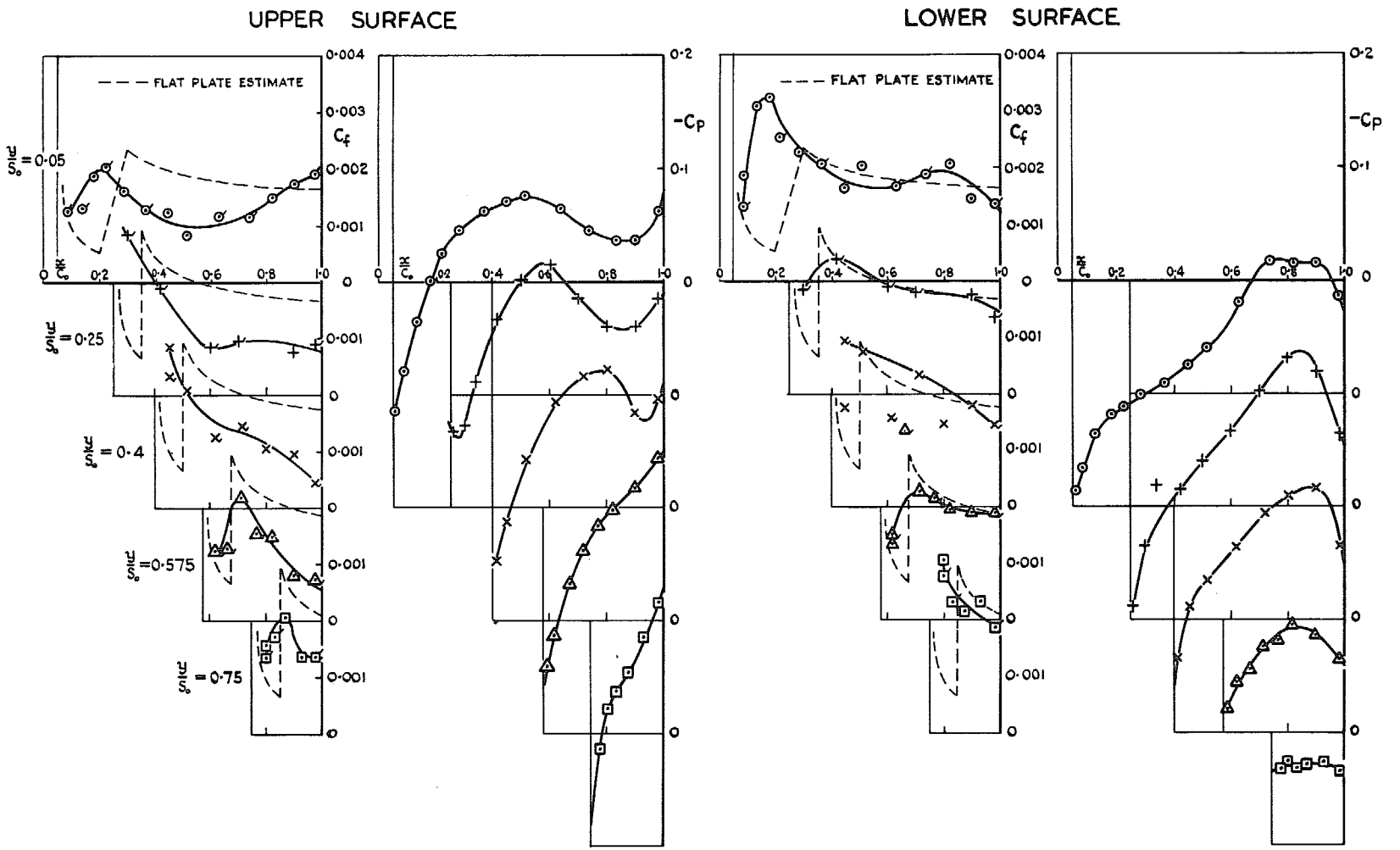

(d) $\alpha = 6°$

FIG. 6 (contd.). Skin friction and pressure coefficients $M = 2{\cdot}6$ $Re_{c_0} = 10^7$.

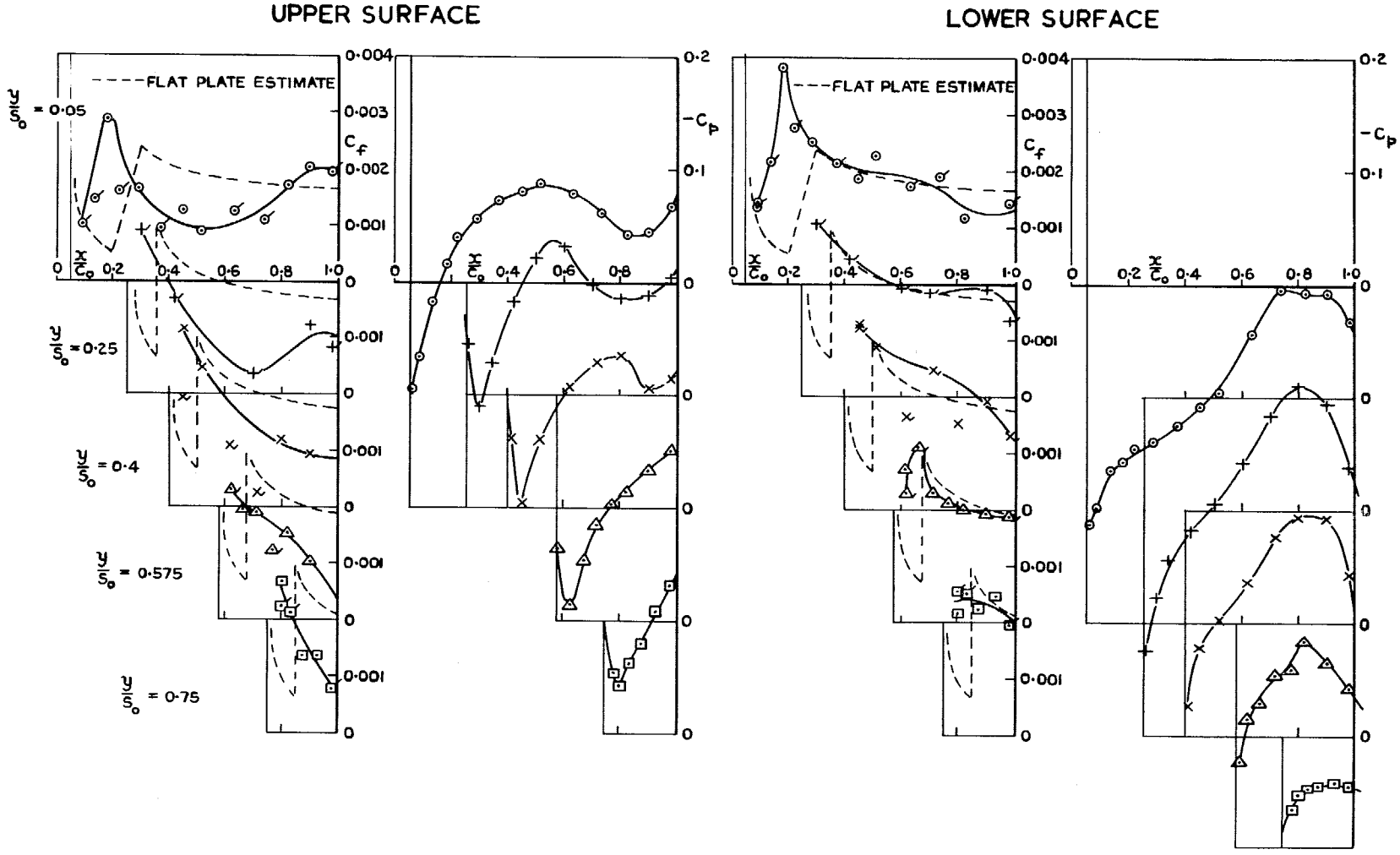

(e) $\alpha = 8°$

FIG. 6 (contd.). Skin friction and pressure coefficients $M = 2{\cdot}6$ $Re_{c_0} = 10^7$.

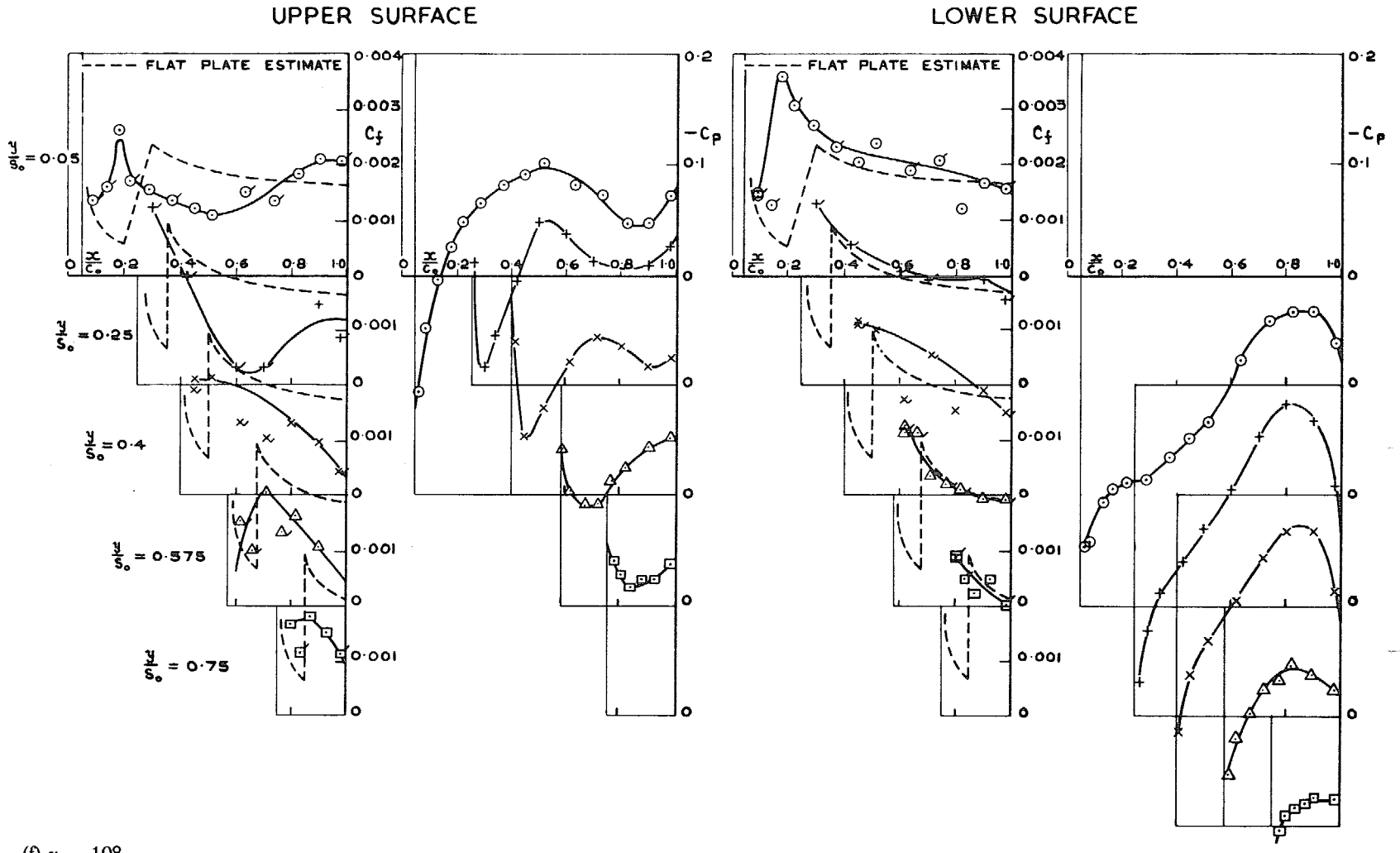

(f) $\alpha = 10°$

FIG. 6 (concl.). Skin friction and pressure coefficients $M = 2{\cdot}6$ $Re_{c_0} = 10^7$.

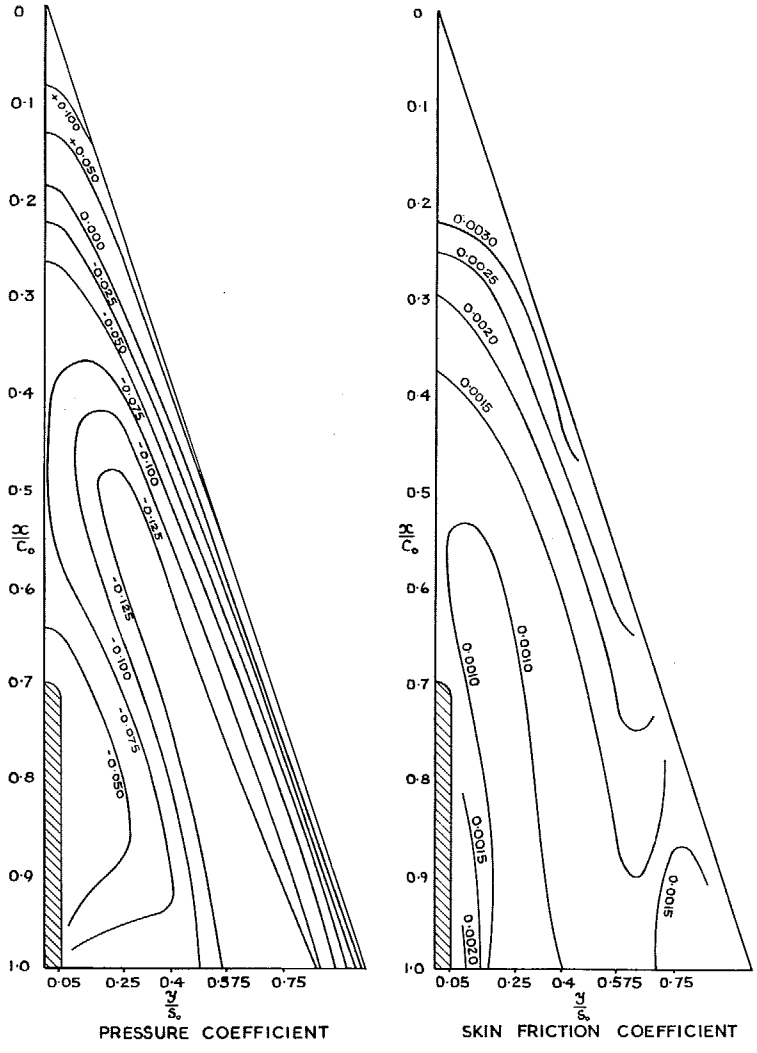

FIG. 7. Contours of skin friction and pressure coefficients at design point $M = 2{\cdot}1$ $\alpha = 5{\cdot}3°$ ($C_L = 0{\cdot}1$) upper surface.

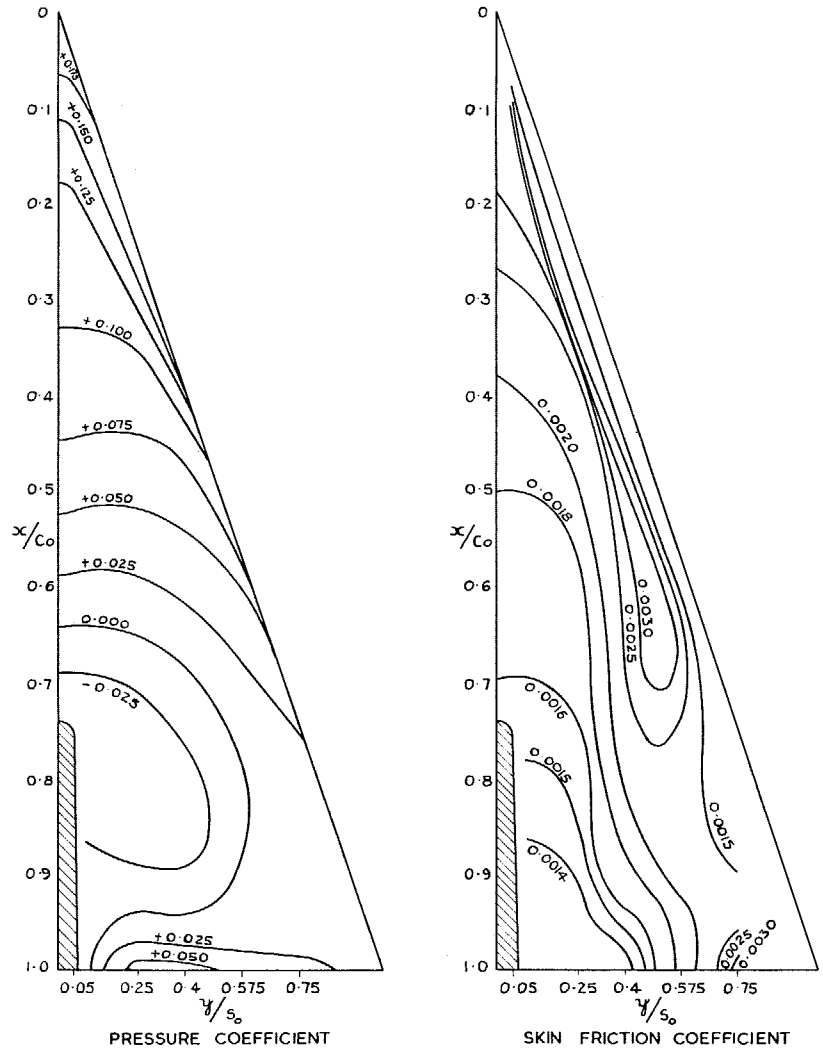

FIG. 8. Contours of skin friction and pressure coefficients at design point $M = 2{\cdot}1$ $\alpha = 5{\cdot}3°$ ($C_L = 0{\cdot}1$) lower surface.

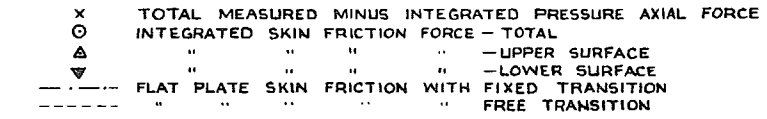

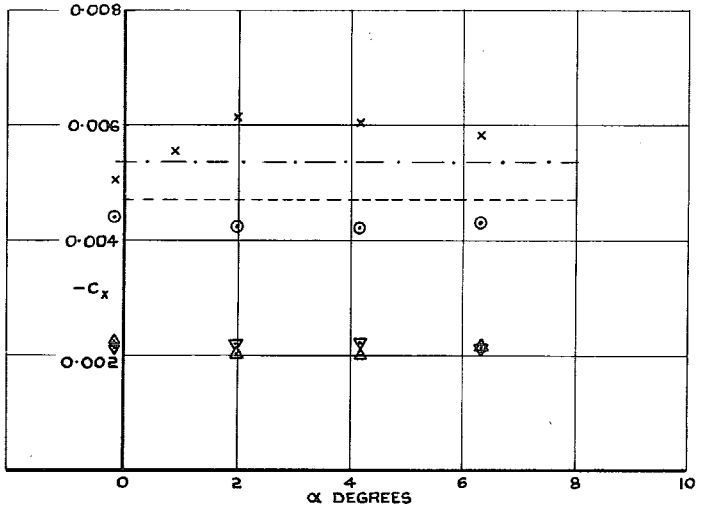

FIG. 9. Axial force coefficient $M = 1{\cdot}5\ Re_{c_0} = 10^7$.

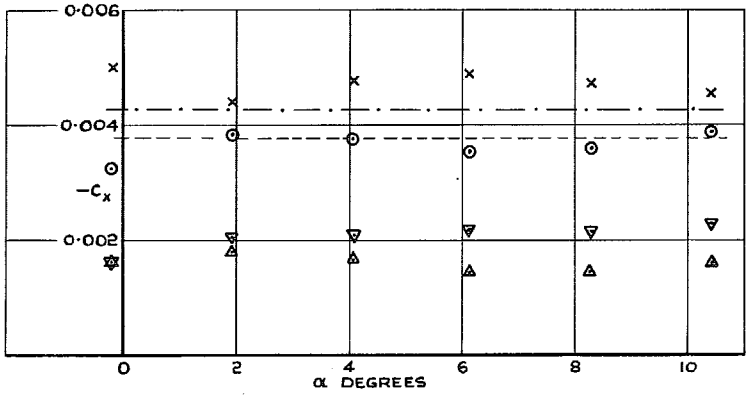

FIG. 10. Axial force coefficient $M = 2{\cdot}6\ Re_{c_0} = 10^7$.

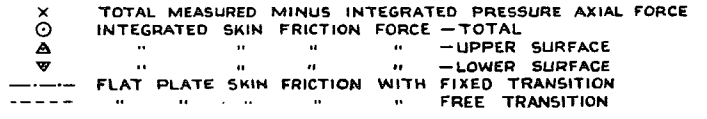

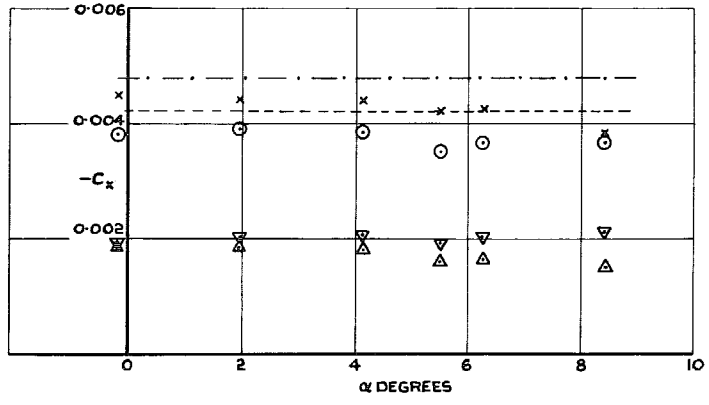

FIG. 11. Axial force coefficient $M = 2{\cdot}1\ Re_{c_0} = 10^7$.

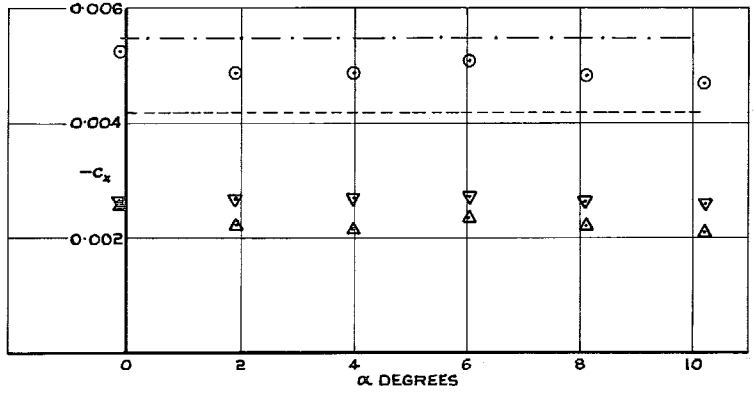

FIG. 12. Axial force coefficient $M = 2{\cdot}1\ Re_{c_0} = 5 \times 10^6$.

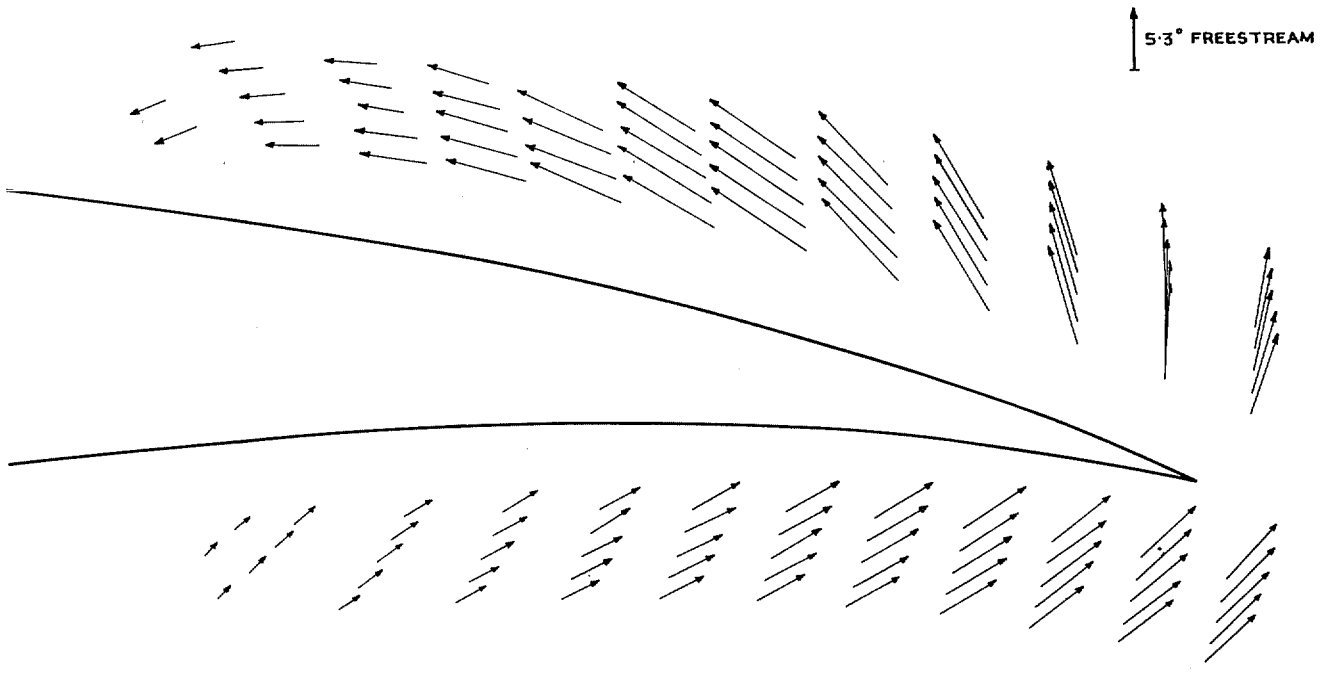

FIG. 13. Cross flow directions for design point $M = 2{\cdot}1$ $\alpha = 5{\cdot}3°$. Station A $x/C_0 = 0{\cdot}667$.

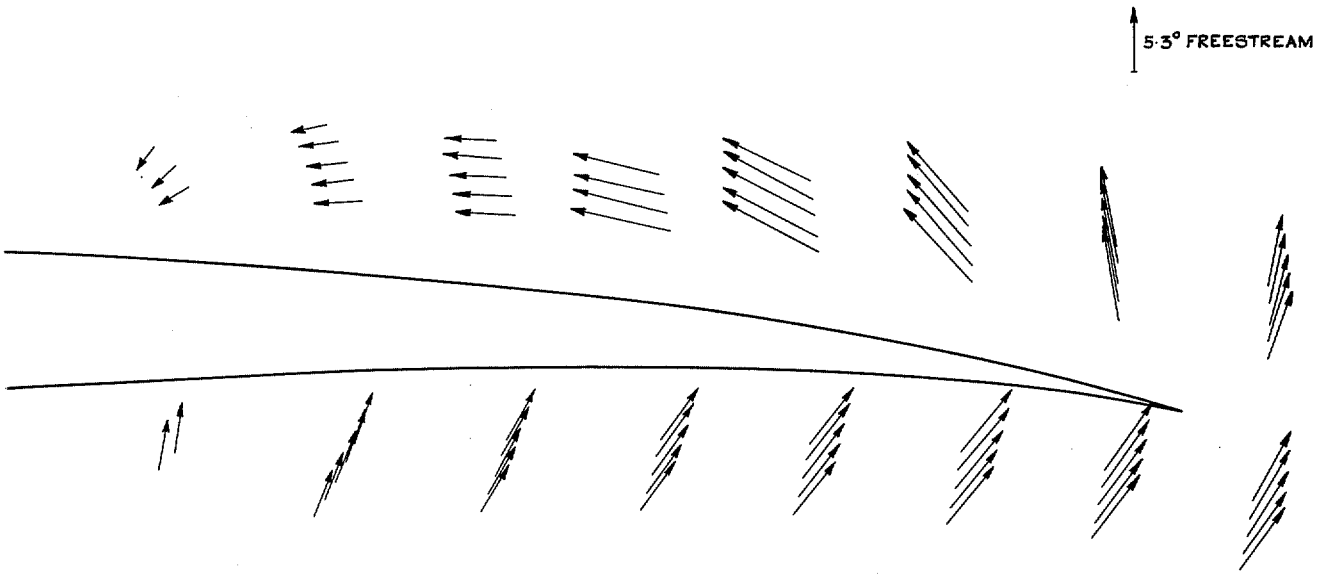

FIG. 14. Cross flow directions for design point $M = 2{\cdot}1$ $\alpha = 5{\cdot}3°$. Station B $x/C_0 = 0{\cdot}8$.

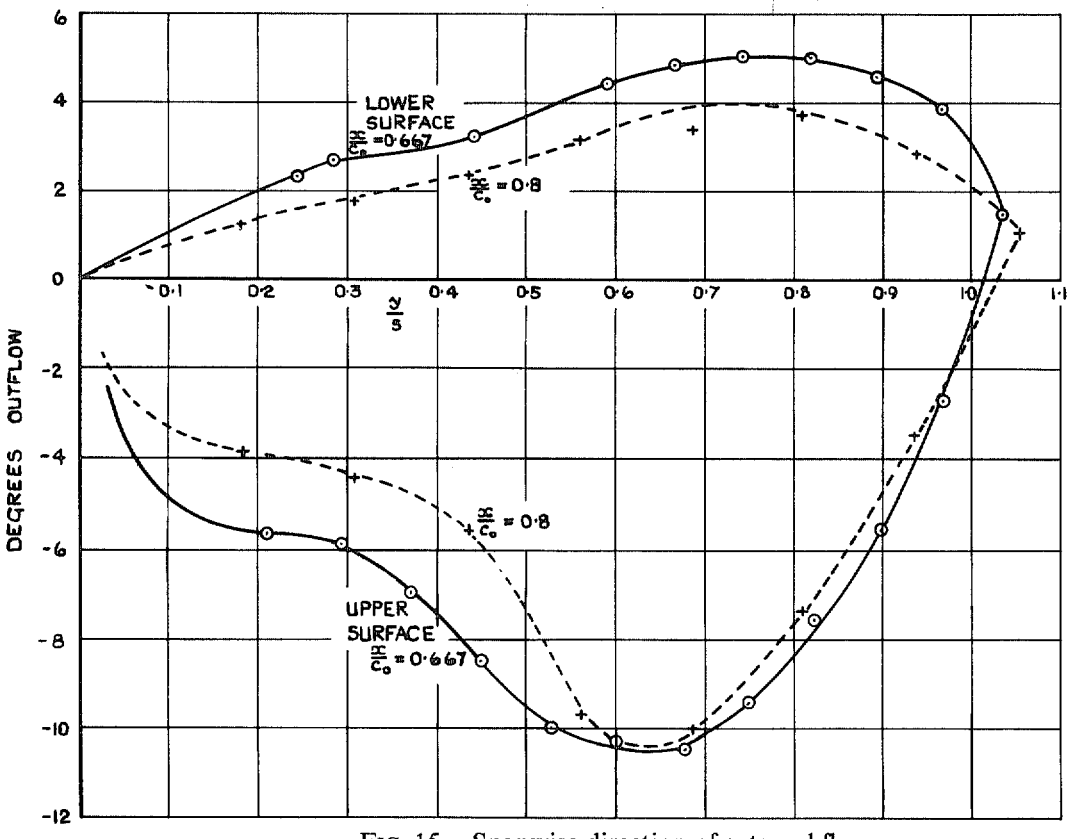

FIG. 15. Spanwise direction of external flow.

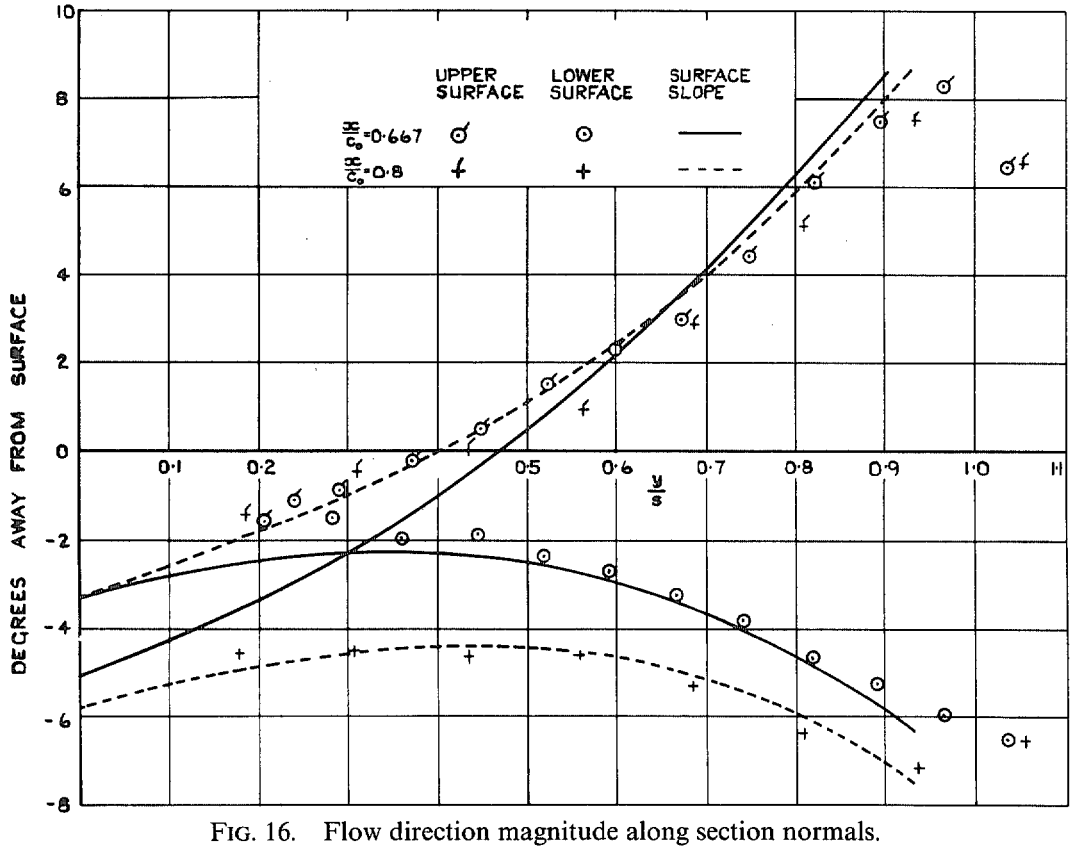

FIG. 16. Flow direction magnitude along section normals.

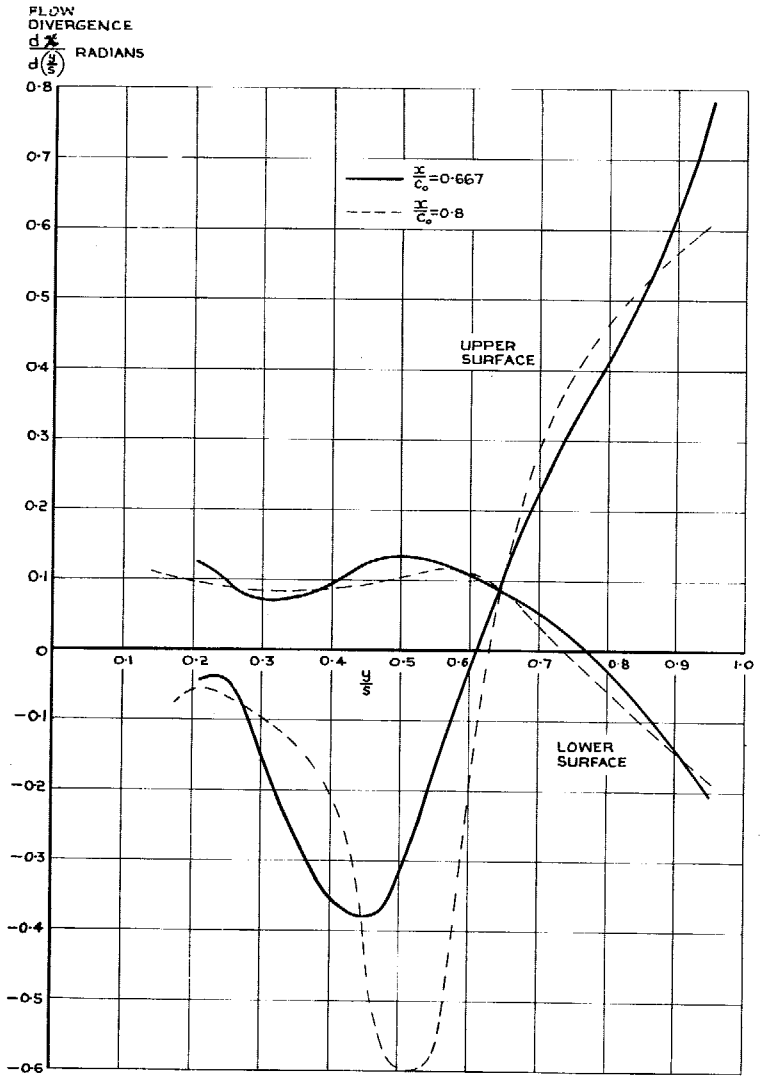

FIG. 17. Divergence of external flow.

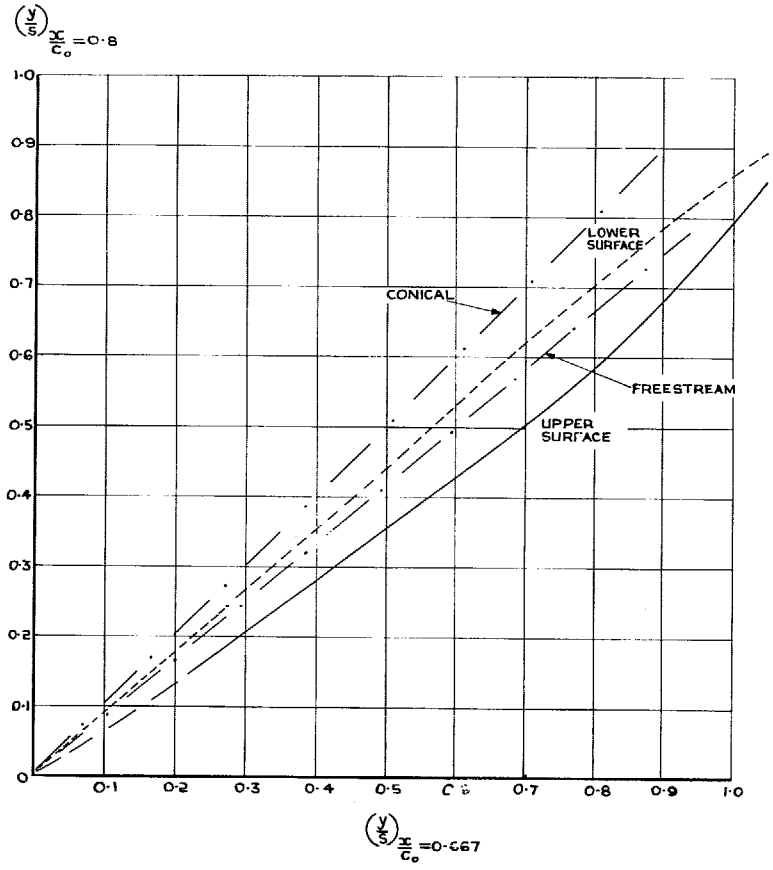

FIG. 18. Relation between spanwise positions of streamlines at the two measuring stations.

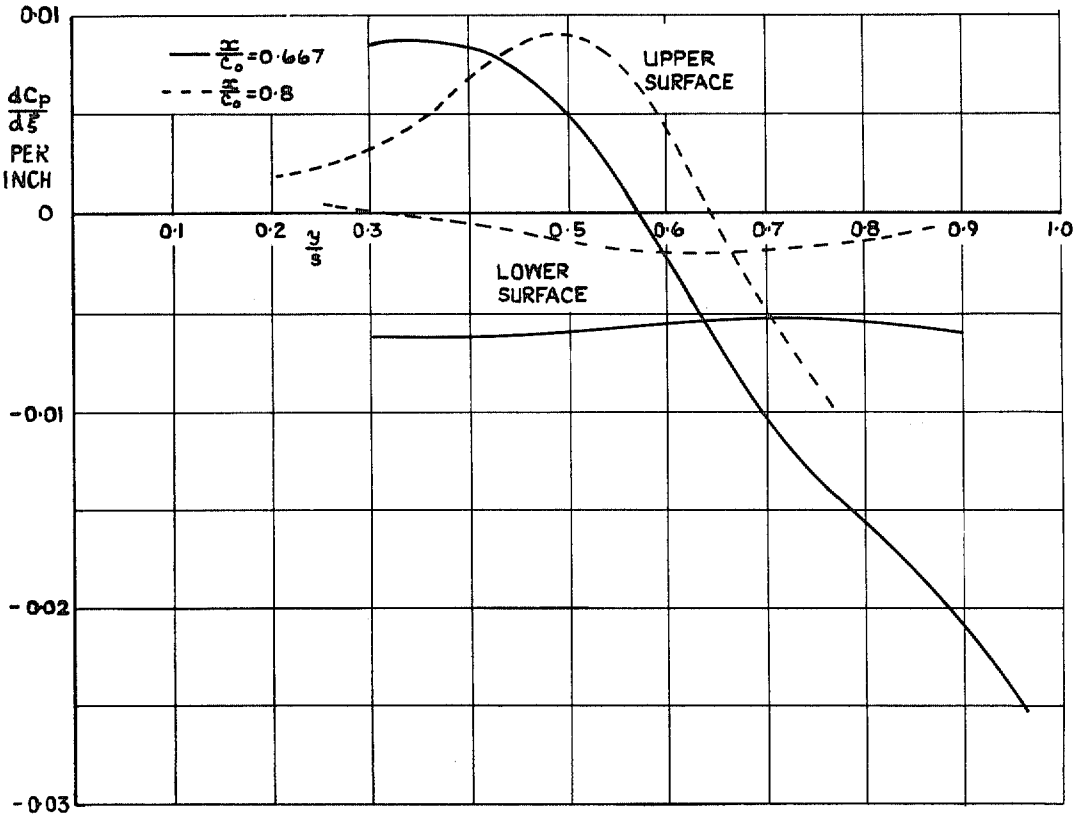

FIG. 19. Pressure gradients along streamlines.

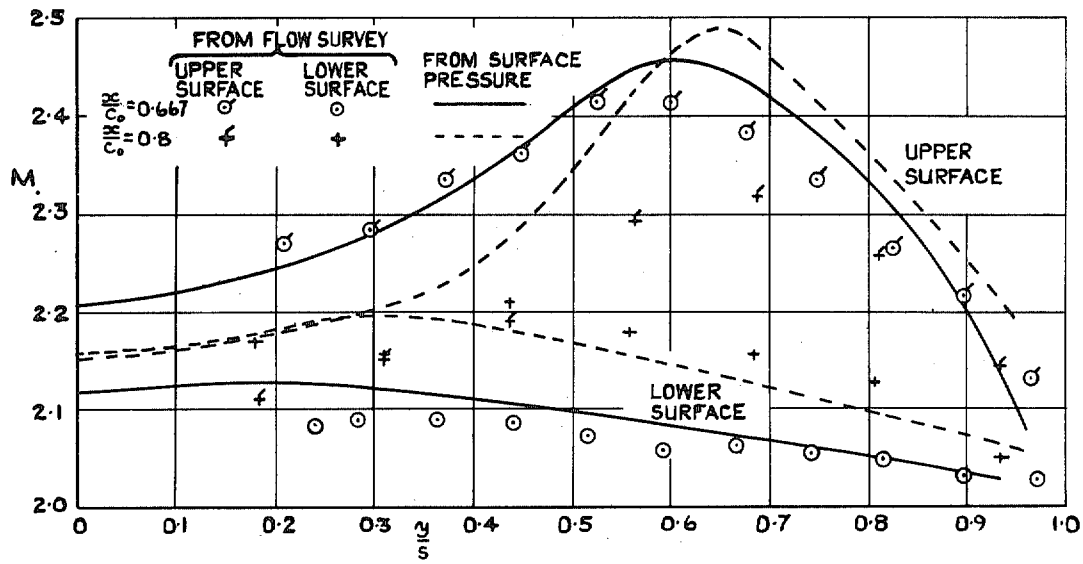

FIG. 20. Mach number of external flow.

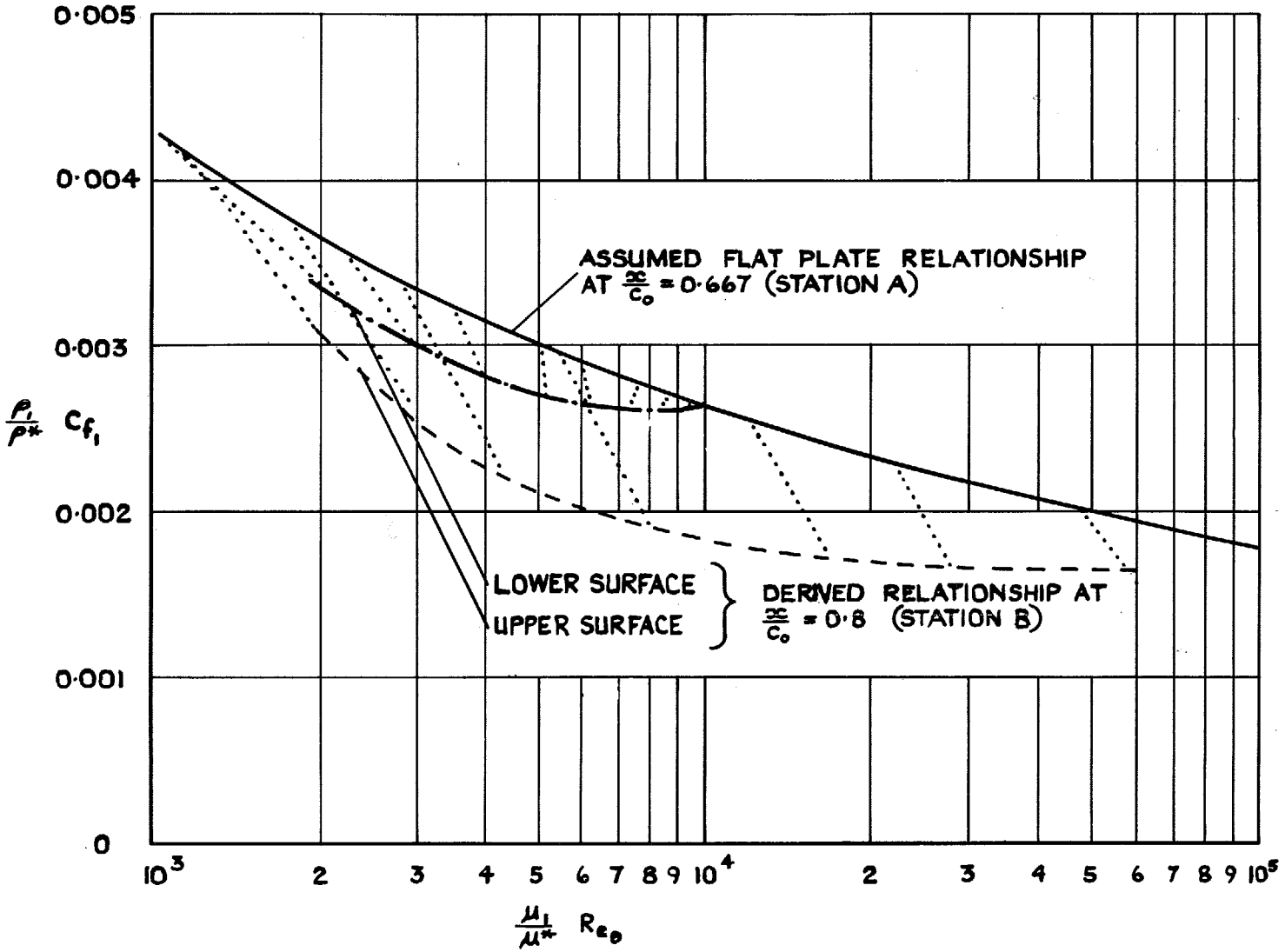

FIG. 21. Derived skin-friction relationships.

Printed in Wales for Her Majesty's Stationery Office by Allens Printers (Wales) Limited
Dd.129527 K.5

Published by
HER MAJESTY'S STATIONERY OFFICE

To be purchased from
49 High Holborn, London w.c.1
423 Oxford Street, London w.1
13A Castle Street, Edinburgh 2
109 St. Mary Street, Cardiff, CF1 1JW
Brazennose Street, Manchester 2
50 Fairfax Street, Bristol 1
258–259 Broad Street, Birmingham 1
7–11 Linenhall Street, Belfast, BT2 8AY
or through any bookseller

S.O. Code No. 23–3501